UNIVERSITA' DEGLI STUDI DI NAPOLI "FEDERICO II"

Dottorato di ricerca in
MORFOLOGIA CLINICA E PATOLOGIA
Dipartimento di Scienze Biomorfologiche e Funzionali

"Understanding the Role of Calcium in Cardiac Arrhythmias Using Mouse Models of Cardiovascular Diseases".

Relatore
Prof. S. Montagnani

Candidato
Dott. Salvatore Mancarella

Correlatore
Prof . Mohamed Boutjdir

Tesi svolta presso: Columbia University Department of Physiology and Cellular Biophysics, and within Molecular and Cellular Cardiology Program at VA New York Harbor Healthcare System, SUNY Downstate Medical Center, New York. USA.

“Understanding the Role of Calcium in Cardiac Arrhythmias Using Mouse Models of Cardiovascular Diseases”.

Year 2007

Index

Acknowledgments

This thesis is the result of three years work and it would never have been possible for me to accomplish this without the help, support and encouragement from many people. Foremost, I wish to express my gratitude to my advisors, Prof. Stefania Montagnani and her assistants Dr. Castaldo and Dr. DiMeglio; to Dr. Mohamed Boutjdir and Dr. Andrew Marks, for giving me the opportunity to achieve the research of this thesis by letting me work in their laboratories at VA NY Harbor Healthcare System and Columbia University. I greatly appreciate the guidance they have given me over the years. The numerous discussions that we have had have been a constant source of inspiration to me. I have benefited from the numerous experts I have had the honor to meet. I want to extend my gratitude to people I have met even before this work began. I am especially grateful to Dr. Piero Anversa, Dr. Michael Artman, with whom I have worked very closely gaining insight in the cardiovascular physiology and electrophysiology. Their never-ending stream of ideas and their passion for research has fired my own enthusiasm. I would like to thank them for their ideas, comments and challenges, all of which have contributed to my professional growth. I have met many interesting people who have made the experience a rich one, not only at work but also on a personal level. I would like to mention two of them in particular: Dr. Baosheng Lee (Regeneron Pharmaceuticals, Inc, New York) for teaching me surgical skills and complex in vivo techniques, and Dr. Douglas Holmes (Medicine and Pediatrics, New York University).

Finally, last but not least, my sincere gratitude goes to my wife Irene for her continuous and unconditional support and encouragement throughout my studies.

Abstract

Increased use of mouse models of cardiac abnormalities are becoming “state of art” tools to understand the mechanism of the cardiac rhythm disorders. Carefully regulated calcium cycling is critical for cardiac function, a variety of ion channels, ATP-dependent pumps, and transporter proteins serve as the major control points of calcium regulation in the heart, including L-type calcium channels and ryanodine receptors (RyR) for calcium. In this thesis, results from 2 genetically modified mouse models are presented: FKBP12.6 knock-out mouse which exhibit stress induced arrhythmia; and alpha1D Knock-out mouse as model of atrial fibrillation which reveals new mechanisms during cell contraction, and heart impulse propagation.

In vivo techniques have been used to study the cardiac phenotype. In addition, single cardiomyocytes were obtained from these mouse models. Calcium transient and ion channels activity were measured, in normal state and in pathological state with the use of optical and patch clamp techniques. New molecules (JTV519) are tested using FKBP12.6 KO mouse to manipulate intracellular calcium preventing cardiac arrhythmias.

The results presented here expands the current knowledge of cardiac physiology, illustrate new mechanisms of heart disease and new pharmacological strategies that could help to reduce disability and death from heart disease and stroke.

Introduction

The cardiac beat disorders

The normal human heart is a strong, muscular pump a little larger than a fist. It pumps blood continuously through the circulatory system. Each day the average heart beats (expands and contracts) 100,000 times and pumps about 2,000 gallons of blood. In a 70-year lifetime, an average human heart beats more than 2.5 billion times (*American Heart Association web site*).

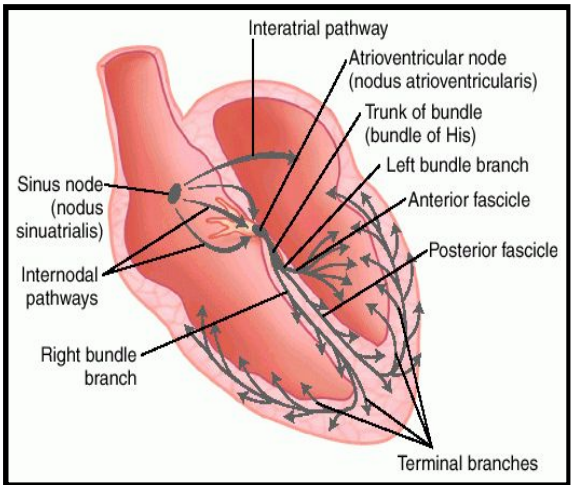

Figure 1. Diagrammatic view of the conducting system (source*: the internet*).

The heart is classically described as a four pumping chambers, right and left atria's, right and left ventricles, it beats when an electrical impulse from the heart's sinoatrial node "SA node" moves through the heart. The normal heart beat sequence, called the "sinus rhythm", begins in the right atrium (RA), (Figure 1), spreads throughout the atria and to the atrioventricular node "AV node". From the AV node, the impulses travel down a group of specialized fibers (the His-Purkinje system) to all parts of the ventricles. This exact route must be followed for the heart to pump properly. As long as the electrical impulse is transmitted normally, the heart pumps and beats at a regular pace. The "Cardiac rhythm disorders" is referred to several disorders that impair the cardiac functions with derangements that vary from mild symptoms to life-threatening complications known as *"arrhythmias"*. Arrhythmias are generally divided into two

categories: ventricular and supraventricular. Ventricular arrhythmias occur in the lower chambers of the heart; it can be rapidly fatal commonly known as sudden cardiac death (SCD). SCD appears to be a degeneration of ventricular fibrillation (VF) during which disorganized contractions of the ventricles fails to eject blood effectively, often followed by a pulseless electrical activity. Often VF is associated with common cardiac diseases, most notably heart failure, in which approximately 50% of patients die from fatal cardiac arrhythmias and is estimated to kill about 600,000 individuals per year in Europe and the United States combined. However, these fatal arrhythmias can also occur in young, otherwise healthy individuals without known structural heart disease.

Supraventricular arrhythmias occur in the area above the ventricles known as atrial fibrillation (AF) it manifest with a disorganized, ineffective quivering caused by chaotic conduction of electrical signals through the upper chambers of the heart. AF is the most common arrhythmia in the population; it is associated with increased mortality in case of mild-to-moderate heart failure. Atrial fibrillation is also associated with other forms of cardiovascular disease, including one or more of the following: congestive heart failure, rheumatic heart disease, coronary artery disease, left ventricular hypertrophy, cardiomyopathy and hypertension. Atrial fibrillation may cause up to a 30% reduction in cardiac output resulting in shortness of breath, fatigue and reduced exercise capacity and a reduction in cerebral blood flow during the fibrillation episode. Formation of blood pools in the chambers can lead to the formation of blood clots that can dislodge and travel to the brain resulting in stroke.

Where do we stand?

Standard antiarrhythmic drug therapy has failed to reduce and in some instances has increased the incidence of SCD. Regarding therapeutic advances in cardiovascular research, Dr. Katz's pose this paradox: at the present time our knowledge of the molecular basis of cardiac electrical activity is increasing by leaps bounds thanks to recombinant DNA technology and patch clamp electrophysiology, but application of this information to the development of effective new therapies for cardiac arrhythmia is decreasing. This paradox finds its explanation in the complexity of the electrical dysfunctions in the intact heart and the disappointment to date of preventive therapy for patient at risk from cardiac arrhythmias [*Katz. al. 1995*].

Impetus for new directions

The nature of the immediate precipitating event that triggers the fatal ventricular tachyarrhythmia at a specific time in an otherwise stable patient remains as the major unanswered question. A result of regulatory guidelines for new drug development, the cost of bringing new drugs into the clinic appear prohibitive to the pharmaceutical industry, discouraging many from seeking solution to the problems of how to treat cardiac arrhythmias and reduce the incidence of sudden cardiac death. However, recent breakthroughs in research on cardiac electrophysiology have enabled us to focus on individual ion channel proteins, the molecules that generate excitatory and repolarizing currents in normal and diseased myocardial cells. Increased understanding of drug-channel protein interaction will ultimately allow us to develop newer and more effective drug to deal with this enormous public health problem [*Spooner et. al. 1995*].

Origin of the heart beat

Cardiac muscle has some similarities to neurons and skeletal muscle, as well as important unique properties. Like a neuron, a given myocardial cell has a negative membrane potential when at rest. Stimulation above a threshold value induces the opening of voltage-gated ion channels and a flood of cations into the cell. When the threshold is met, an action potential initiates. This causes the positively charged ions to enter the cell [depolarization]. Like skeletal muscle, depolarization causes the opening of voltage-gated calcium channels and entry of Ca^{2+} from the t-tubules. This influx of calcium causes calcium-induced calcium-release (CICR) from the sarcoplasmic reticulum, and the increase in myoplasmic free Ca^{2+} concentration causes muscle contraction. After a delay (the absolute refractory period), potassium channels reopen and the resulting flow of K^{+} out of the cell causes repolarization to the resting state. The process whereby an action potential triggers a myocyte to contract is known as excitation-contraction coupling (ECC) (Figure 2).

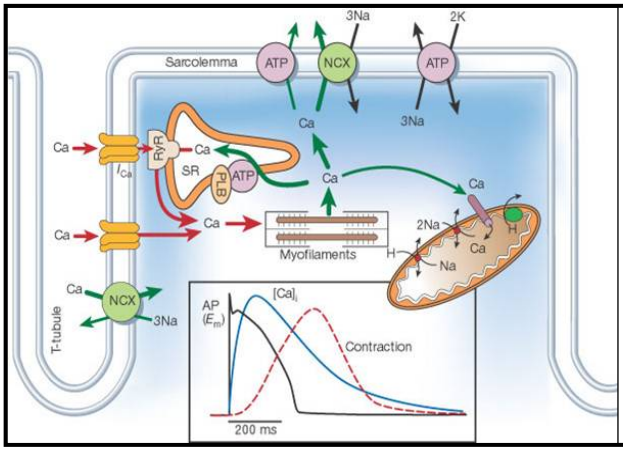

Figure 2. Ions fluxes generate the heart beat. A small amount of calcium enters cells through the L-type calcium channel (LTCC), triggering release of a much larger amount of calcium from the sarcoplasmic reticulum (SR) through ryanodine receptors (RyR). Most of the calcium is pumped back into the SR by SERCA2a, and the rest is extruded from the cell by the NCX. Calcium efflux must balance calcium influx. *Bers DM Nature **415**, 198-205 (2002).*

Role of calcium in cardiac arrhythmia

As is shown in figure 2 calcium is central during the ECC and CICR of a single cell in the heart. Alteration in intracellular calcium homeostasis plays an important role in the development of the heart beats and ventricular tachyarrhythmia in the failing heart as well as in some inherited syndromes leading to SCD. Congenital Ca^{2+} handling abnormalities in the heart include defective function of the ryanodine receptor 2 (RYR2) in catecholaminergic polymorphic VT (CPVT), ankyrin-B mutation in long-QT syndrome, calsequestrin (CSQ) mutation, and intracellular calcium alteration. The role of abnormal calcium signaling in the genesis of cardiac arrhythmias has generated considerable interest over the past three decades; because of this key role, all aspects of calcium cycling are inviting targets for antiarrhythmic strategies.

Here I am going to focus on two distinct components of the calcium cycling components, both are calcium channels: 1) the cardiac ryanodine receptor (RYR-2), an intracellular calcium channel localized in the sarcoplasmic reticulum that once opened release the calcium stored in the SR starting the contraction, it seems that mutation of this channel are associated with lethal forms of arrhythmias like stress induced arrhythmias. 2) The alpha 1D calcium channel, It is a relatively new calcium channel that has been discovered to be expressed in the atria's, up to date there is no evidences of the relative contribution of this channel in the heart, but it is very interesting the fact that mouse model of α1D genetically deleted (α1D KO)are prone to arrhythmias.

Part I
“The FKBP12.6 KO mouse model”.

Overview of the ryanodine receptor

Three mammalian isoforms of ryanodine (RyR), each encoded by a specific gene, have been identified and cloned; they are named RYR1, RYR2, and RYR3. RYR1 is expressed predominantly in skeletal muscle, RYR2 is expressed predominantly in cardiac muscle, and RYR3 is expressed in the brain and other non-muscle as well as muscle tissues. RyR single channel are homotetramers 2.4 x 10^6 kDa located in the SR membrane. Each subunit (Figure 3) is structurally similar along the three isoforms, ~565 kDa with 6 putative membrane-spanning domains that include the pore region and a large cytoplasmic N-terminal domain, termed the "foot structure" that spans the gap between the SR and transverse tubule (T-tubule). Several of the channel modulators bind to this cytoplasmic scaffold domain such as, calmodulin, FKBP12.6 [1,2], PKA [3], phosphatases1 and 2A (PP1 and PP2A) [3], and sorcin. Triadin and junctin are involved in the membrane anchoring of RyR, and calsequestrin is involved in high-capacity intracellular calcium buffering.

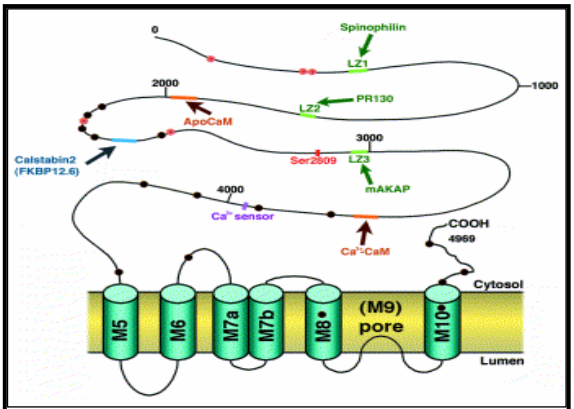

Figure 3. Structural domains of the cardiac ryanodine receptor and satellite proteins. The primary structure of a cardiac ryanodine receptor and binding domains of protein phosphatases 1 and 2A, protein kinase A, calmodulin and FKBP12.6 are indicated

Human arrhythmia disease associated with RYR mutations

Two clinically distinct forms of SCD in children and young adults have recently been linked to autosomal-dominant mutations in RyR2 [4,5]. These disorders, known as catecholaminergic polymorphic ventricular tachycardia (CPVT) and arrhythmogenic right-ventricular dysplasia/cardiomyopathy (ARVD/C) type 2 share the clinical characteristics of exercise-induced ventricular arrhythmias and sudden cardiac death [5-8]. CPVT, a rare disorder, has a very high mortality rate (up to 50% by the age of 30 years)[5,9], sudden cardiac death can be the presenting symptom. In 1999, Swan *et al*. [10] linked the disorder to the *hRyR2* gene locus in two Finnish families. Subsequently, more than 16 missense mutations in *hRyR2* have been linked to CPVT [6-8,11]. ARVD/C is characterized by the progressive replacement of right-ventricular free wall with fibrous and fatty tissue [12]. Linkage studies have identified eight chromosomal loci in families with the disorder. ARVD/C type 2, caused by mutations in the *hRyR2* gene, is characterized by a unique association with exercise-induced arrhythmias [7]. ARVD/C mutations in RyR2 were mapped to the mutation hotspot regions linked to CPVT, and the analogous regions in RyR1 were linked to malignant hyperthermia and central core disease. The associations with exercise and stimulation of the sympathetic nervous system are notable because mutations in RyR2 are also linked to exercise and stress-induced sudden cardiac death in the absence of any structural heart disease. Recent findings in mice with recombinant CPVT-mutant RyR2 channels have contributed to a better understanding of this mechanism [13]. Mutant forms of RyR2 found in CPVT patients [5] have a decreased binding affinity for FKBP12.6 [13], which causes increased RyR2 activity after PKA phosphorylation. Six distinct and structurally unrelated RyR2 missense mutations found in

CPVT carriers all decrease the binding affinity of FKBP12.6 for RyR2 [3,14]. This finding suggests a common mechanism for the RyR2 gain-of-function defect associated with exercise-induced arrhythmias [3,14], because DADs and arrhythmia triggers occur in conjunction with diastolic sarcoplasmic reticulum (SR) Ca^{2+} leak in heart failure in which RyR2 are chronically depleted of FKBP12.6 [15], and CPVT missense mutations decreases the FKBP12.6 binding affinity to RyR2 [3,14].

Outline of RYR project

To elucidate the role of RYR-2 during arrhythmia we have used engineered mice with genetically deleted *FKBP12.6* (*FKBP12.6* -/-) known to be prone to stress induced arrhythmia. We investigate the cellular mechanism that leads to the disease and the role of calcium as a trigger for the arrhythmia. We hypothesized that *FKBP12.6* depletion from the RyR2 complex during β-adrenergic stimulation (β-AR stimulation) constitutes a common mechanism of arrhythmia initiation for catecholaminergic VT. *FKBP12.6* deficiency may be directly responsible for promoting dynamic electrical tissue heterogeneity during β-AR stimulation leading to VT. Thus we examined how RyR2 function is affected in absence of *FKBP12.6* and how calcium homeostasis is changed in the heart at single cell level.

The animal model used in this study was also a valuable tool to study a new cardioprotective[16-18] drug, JTV-519 which blocks Na^+ current and inwardly rectifying K^+ current and inhibits Ca^{2+} current. However, its role in atrial electrophysiology is unknown. Our hypothesis is that JTV would facilitate the association of *FKBP12.6* to RYR2 in diseased heart, for this second aim we used haploinsufficient *FKBP12.6*$^{+/-}$ mouse expressing a reduced amount of protein (50% *FKBP12.6* reduction) that associate to

RYR2 therefore still developing arrhythmias. We also screened for more efficient and target specific JTV519-derivates.

Results

FKBP12.6 KO cardiac phenotype and JTV509 treatment

JTV519-treated WT, haploinsufficient *FKBP12.6*$^{+/-}$ and *FKBP12.6*$^{-/-}$-deficient mice did not exhibit ventricular tachycardia (VT) under resting conditions, in agreement with previous results.[5,9] Isoproterenol (ISO) (0.5 mg·kg^{-1} i.p.) produced a significant increase in maximal heart rate in all groups: WT, 750 ± 42 min^{-1}; *FKBP12.6*$^{+/-}$, 748 ± 38 min^{-1}; or *FKBP12.6*$^{-/-}$, 747 ± 44 min^{-1} (each $P < 0.05$ compared with baseline). JTV519 treatment (7-day continuous infusion of 0.5 mg·kg^{-1}·hr^{-1} via osmotic minipump) did not affect the increase in heart rate due to ISO: *FKBP12.6*$^{+/-}$ plus JTV519, 732 ± 45 min^{-1}; or *FKBP12.6*$^{-/-}$ plus JTV519, 728 ± 52 min^{-1} (each $P < 0.05$ compared with baseline).

WT, *FKBP12.6*$^{+/-}$, and *FKBP12.6*$^{-/-}$ mice underwent programmed electrical stimulation (PES) to test for arrhythmia susceptibility. Compared with untreated animals, JTV519-treated conscious *FKBP12.6*$^{+/-}$ and *FKBP12.6*$^{-/-}$ mice revealed no significant differences in resting electrocardiographic parameters like PR, QRS intervals, and rate-corrected QT interval), Including heart rate* (RR interval). However, PES reproducibly induced bidirectional VT in *FKBP12.6*$^{+/-}$ mice but not in WT controls (Figure 4 *A* and *C*). Simultaneous epicardial monophasic action potential (MAP) recordings showed that PES-induced sustained or nonsustained VT (sVT or nsVT, respectively) correlated closely with MAP instability (Figure 4*A* and *B*). After ISO treatment, pacing at short cycle lengths (CLs) or premature coupling intervals (S1–S2; S1–S2–S3) resulted in MAP alternans, which continued after pacing stopped (Figure 4*B*). Sustained MAP alternans occurred in 100% of sVT in *FKBP12.6*$^{+/-}$ and *FKBP12.6*$^{-/-}$ mice but never in WT control (Figure 4*C*). Sustained VT was observed in 86% of the *FKBP12.6*$^{+/-}$ mice, which was not significantly

different from *FKBP12.6*$^{-/-}$ knockout mice (Figure 4*C*); however, sVT was never observed in WT mice, confirming earlier results. [13,19]

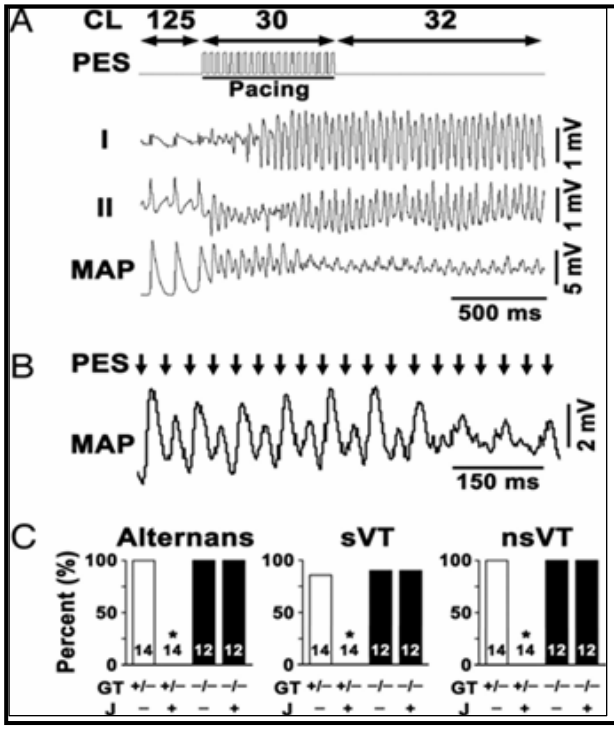

Figure 4. *FKBP12.6* deficiency causes pacing-induced bidirectional VT and MAP alternans, which are prevented by JTV519. (*A*) Representative lead I and II ECG tracings and simultaneous left ventricular epicardial MAP recording from a placebo-treated *FKBP12.6*+/– mouse during overdrive pacing at CL 30 ms as documented by PES trace. Pacing triggered sustained bidirectional VT, as evidenced by simultaneous ECG and MAP recordings shown at higher resolution in *B*. Pacing stimuli (arrows) induced MAP alternans that continued after cessation of pacing in placebo-treated *FKBP12.6*+/– mice (CL 32 ms). (*C*) Bar graphs summarizing simultaneous occurrence of bidirectional MAP alternans (*Left*) and sustained VT (sVT) (*Center*) or nonsustained VT (nsVT) (*Right*) arrhythmias in placebo-treated (J–) or JTV519-treated (J+) *FKBP12.6*+/– (open bars) or *FKBP12.6*–/– (filled bars) mice during ISO stimulation (0.5 mg·kg−1 body weight). Mouse numbers and dimensions are as indicated. sVT, >10 beats (*Center*); nsVT, 3–10 arrhythmogenic beats (*Right*). GT, genotype.

FKBP12.6$^{+/-}$ mice pretreated for 1 week with JTV519 (0.5 mg·kg^{-1}·hr^{-1}) developed significantly fewer exercise-induced arrhythmias ($P < 0.05$) (Figure 4*C*). In contrast, JTV519 caused no significant reduction of arrhythmias in *FKBP12.6*$^{-/-}$-deficient mice, indicating that *FKBP12.6* is required for the antiarrhythmic actions of JTV519 (Figure 4*C*). JTV519-treated *FKBP12.6*$^{+/-}$ mice exhibited no sustained MAP alternans (Figure 4*C*), indicating that JTV519 effectively increased the threshold for arrhythmia inducibility and MAP alternans. Arrhythmias and MAP alternans also occurred spontaneously in *FKBP12.6*$^{+/-}$ and *FKBP12.6*$^{-/-}$ mice, and were never observed in WT mice (Figure 5). JTV519 inhibited the occurrence of spontaneous arrhythmias and MAP alternans only in *FKBP12.6*$^{+/-}$ mice but not in *FKBP12.6*$^{-/-}$ mice (Figure 5*B*).

Experiment in the heart (open chest procedure)

To further test the hypothesis that *FKBP12.6* deficiency promotes dynamic electrical tissue heterogeneity during β-AR stimulation, we positioned two MAP electrodes at a fixed distance of 4 mm apart on the left ventricular free wall. During sVT progression, *FKBP12.6*$^{+/-}$ mice exhibited a phase reversal of MAP alternans in the absence of pacing (Figure 5). Because the surface MAP traces reflect the integrated electrical activity of intramural and epicardial cells, 3D optical mapping would be necessary to further differentiate between arrhythmic mechanisms of focal delay after depolarization (DAD) activation versus automatic focus or breakthrough of reentrant waves. However, studies using optical mapping techniques have shown that discordant action potential alternans representing significant electrical instability precedes ventricular fibrillation. [20] The fact that we observed discordant MAP alternans in *FKBP12.6*-deficient mice suggests that both spatial MAP heterogeneities and local MAP instabilities create a dynamic substrate for arrhythmias, none of which were observed in WT mice or *FKBP12.6*$^{+/-}$ mice after JTV519 treatment.

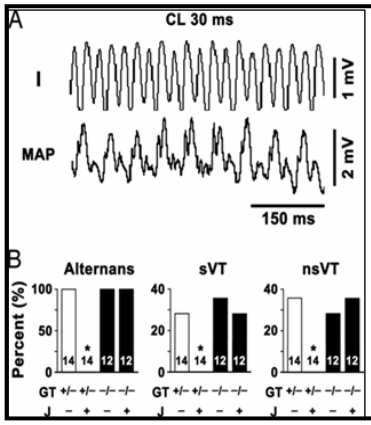

Figure 5. Spontaneous bidirectional VT and MAP alternans in a *FKBP12.6*+/– mouse (no pacing). (*A*) Simultaneous, representative ECG lead I tracing and left ventricular epicardial MAP recording from a placebo-treated *FKBP12.6*+/– mouse during early phase of sVT. CL, cycle length. Bidirectional ECG QRS alternans and MAP alternans are closely correlated. (*B*) Bar graphs summarizing alternans (*Left*), sVTs (*Center*), or nsVTs (*Right*) in placebo-treated (J–) or JTV519-treated (J+) *FKBP12.6*+/– (open bars) or *FKBP12.6*–/– (filled bars) mice during ISO stimulation. GT, genotype.

Calcium dynamics in single ventricular myocytes

To elucidate calcium dynamics and mechanisms of arrhythmia in *FKBP12.6* engineered mice and gain insight on JTV519 action at cellular level we conducted studies in single isolated cardiac myocytes. Pilot experiments were necessary to establish the best approach of how to study calcium dynamic in our mouse model; since we cannot stimulate

arrhythmia/fibrillation in a single cell (arrhythmia in most cases is a multicellular phenomenon). It is now known that RyR2 open probability is affected by the calcium content in the SR, greater SR Ca^{2+} loading increases the probability that RYR2 will open while less complete loading leads to less RyR2 open probability.[4] We showed with single channel experiment that RYR-2 without *FKBP12.6* had alteration in the opening probability (gating) we than designed experiments to over-load the SR Ca^{2+} content and observe (measure) how calcium exit from the SR through RYR2 with and without *FKBP12.6*. Left ventricular myocytes were isolated with enzymatic digestion from three groups of mice (for these experiments mice were not treated with JTV519 neither injected with ISO), cells morphology was unchanged among the groups. Subsequently myocytes were loaded with fura-2 (10 mmol/L for 30 min). Calcium transient and contractions were evoked by electrical field stimulation. Cells were stimulated while continuously superfused in Tyrode`s solution enriched with (ISO 1 mmol/L) to simulate the high level of epinephrine, typical of an emotional stress situations.

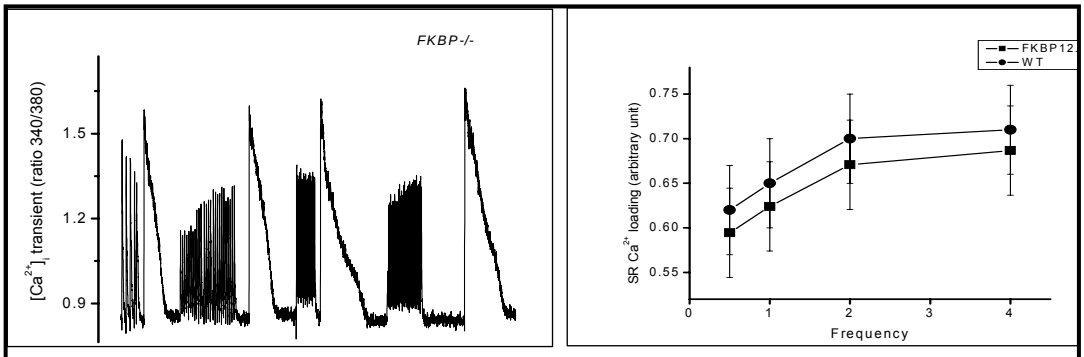

Figure 7. Relationship between SR Ca^{2+} content and sarcolemmal Ca^{2+} fluxes. A,Original data. Trace shows measurements of $[Ca^{2+}]_i$.transient evoked by electrical stimuli followed by a Caffeine $[Ca^{2+}]_i$.transient (10 mmol/L), that empty the SR. Ca^{2+} content for each of the three exposures to 10 mM caffeine in B. panel representing average result of Caffeine $[Ca^{2+}]_I$ transient amplitude after electrical stimulation at three different frequencies.

Firstly we asses how SR Ca^{2+} loading is affected by intracellular calcium, for this purpose myocytes were stimulated at different and increasing frequency allowing few second of rest in between the different frequencies, during the rest period rapid application of caffeine cause the release of the total SR Ca^{2+} content. The SR Ca^{2+} loading increased proportionally to the frequency applied (we consider the amount of Ca^{2+} released coming totally from the SR since calcium influx was blocked by the absence of extra cellular Na^{+} and Ca^{2+}). The amount of calcium stored in the SR was higher in the cell stimulated at 8 Hz than the same cell stimulated at 4 Hz (9.95% increase), we conclude that, the SR Ca^{2+} load is not a fixed amount but it is subject to the amount of citoplasmatic calcium (Figure 7) and this result was valid also in those cells where *FKBP12.6* was genetically deleted.

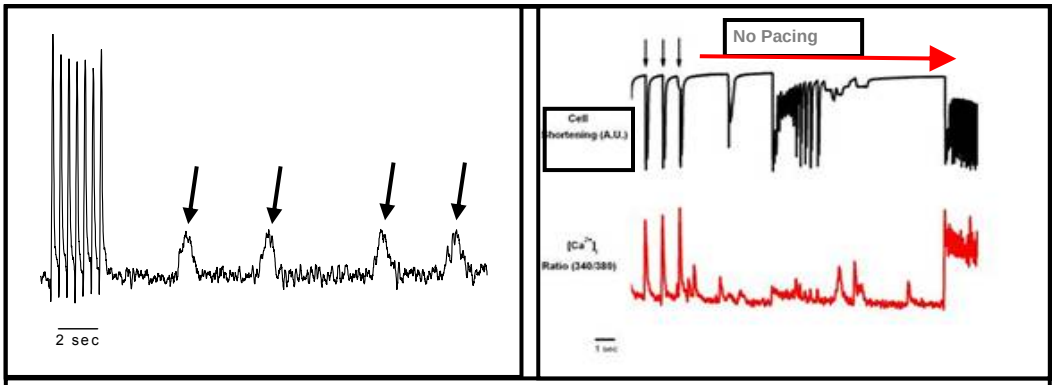

Figure 8 Aftercontractions induced in presence of isoproterenol (1 μmol/L) in isolated myocytes (arrow heads on the left). A train of 20 field-stimulated contractions (last three are shown) in a FKBP -/- myocytes (right) induce an aftercontractions. After exposure to 1 μmol/L isoproterenol (Iso) the same protocol results in an aftercontraction (arrow). In both cases, the stimulation frequency was 0.5 Hz and $[Ca^{2+}]_o$=2 mmol/L.

The SR Ca^{2+} overload is returned to the cytoplasm and extracellular environment if the cell is not electrically stimulated, a phenomenon described as spontaneous Ca^{2+} release. The Ca^{2+} released from the SR through RYR2 was dependent from RYR2 gating properties, Ca^{2+} released spontaneously (i.e., calcium waves) was able to start mechanical contraction-like activity (Figure 8).

We then test if increasing the SR Ca^{2+} loading has a different outcome in our mouse model were we know the RyR2 gating is defective because *FKBP12.6* deprived. We isolated

Programmed field stimulation in the presence of 1 μM ISO was followed by a pause, to monitor for aberrant intracellular Ca^{2+} release events and associated after-contractions (AFCs)[21]. At 0.5 s^{-1} pacing frequency, aberrant Ca^{2+} release and AFCs were observed in <1% of WT, *FKBP12.6*$^{+/-}$, or *FKBP12.6*$^{-/-}$ cardiomyocytes in the presence of 1 μM ISO. Pacing at higher frequencies increased aberrant diastolic Ca^{2+} release and AFCs in 92% of *FKBP12.6*$^{+/-}$ and in 95% of *FKBP12.6*$^{-/-}$ cardiomyocytes at 6 s^{-1} (show calcium aberrant in WT and KO). Previously, we reported that rapid pacing combined with β-AR

stimulation induced DADs in *FKBP12.6*$^{-/-}$ cardiomyocytes [13]. It is therefore likely that these DADs are triggered by aberrant intracellular Ca^{2+} release in the setting of β-AR stimulation and rapid pacing. 30 to 45 minutes preincubation of haploinsufficient *FKBP12.6*$^{+/-}$ cardiomyocytes with 1 μM JTV519 significantly reduced the number of aberrant diastolic Ca^{2+} release events and AFCs after rapid pacing in *FKBP12.6*$^{+/-}$, but not *FKBP12.6*$^{-/-}$, knockout cardiomyocytes ($P < 0.05$) (Figure 9*B* and *D*). Application of caffeine indicated that SR Ca^{2+} store content was significantly reduced by 9 ± 0.3% or 10 ± 0.4% in ISO-treated *FKBP12.6*$^{+/-}$ and *FKBP12.6*$^{-/-}$ cardiomyocytes compared with WT (1-Hz preconditioning; $P < 0.05$) (Figure 9*E*), indicating that *FKBP12.6* deficiency promotes a net SR Ca^{2+} leak during β-AR stimulation.

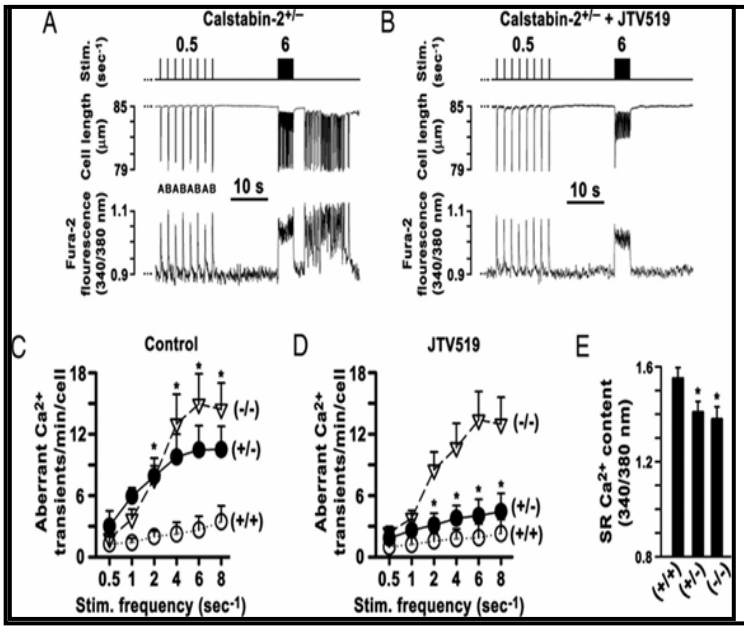

Figure 9. *FKBP12.6* deficiency causes aberrant diastolic Ca2+ release and after-contractions (AFCs) that are prevented by JTV519. (*A*) Alternating (indicated by "A"/"B") intracellular Ca2+ transients and AFCs in *FKBP12.6*+/– cardiomyocyte paced at 0.5 Hz and aberrant Ca2+ release events after 6-Hz pacing. (*B*) JTV519 treatment prevented intracellular Ca2+ oscillations and AFCs in *FKBP12.6*+/– cardiomyocytes after rapid pacing. (*C*) Ca2+ oscillations (min−1 cell−1) are significantly increased at higher pacing rates in *FKBP12.6*+/– or *FKBP12.6*–/– cardiomyocytes compared with WT. (*D*) JTV519 treatment significantly decreased aberrant Ca2+ oscillations in heterozygous *FKBP12.6*+/–, but not *FKBP12.6*–/–, cardiomyocytes. (*E*) SR Ca2+ load measured by local caffeine application was significantly reduced in *FKBP12.6*-deficient cardiomyocytes.

To prove our hypothesis that PKA phosphorylation induce *FKBP12.6* to dissociate, myocytes enriched suspension was treated with isoproterenol, we also investigate if the presence of the new compound JTV519 was able to prevent the *FKBP12.6*-RYR2

complex from dissociating even after phosphorylation and prevent calcium aberrant events. Incubation of isolated cardiomyocytes with ISO for 30 min in the presence of sodium fluoride (1 mmol/L) resulted in maximal RyR2 PKA phosphorylation and significant depletion of *FKBP12.6* from the RyR2 complex (Figure 10*A*). JTV519 significantly increased *FKBP12.6* binding to PKA- phosphorylation RyR2 in *FKBP12.6*$^{+/-}$ cardiomyocytes (Figure. 10*B*). Diastolic SR Ca^{2+} release may activate a Ca^{2+}-dependent transient inward current (I_{TI}) that triggers DADs in *FKBP12.6*$^{-/-}$ cardiomyocytes.[13] Calcium waves originate from random point and propagate throughout the cell as calcium waves that can be visualized in fluo-4 loaded cells (Figure11).Using combined confocal Ca^{2+} imaging and patch-clamp (Figure 12*A*), a depolarizing step after preconditioning and stimulation with 1 μM ISO revealed no aberrant Ca^{2+} release events in WT cardiomyocytes. However, repeating the same protocol during ISO stimulation in *FKBP12.6*$^{+/-}$ cardiomyocytes promoted Ca^{2+} sparks and Ca^{2+} waves (Figure 12*B*), which coincided with the depolarizing I_{TI} and thus are a potential source of DADs and electrical instability (8).

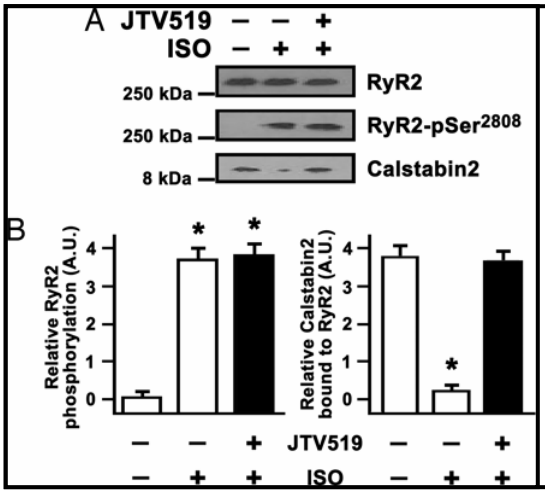

Figure 10. JTV519 increased *FKBP12.6* binding to RyR2 in cardiomyocytes during β-AR stimulation. (*A*) RyR2 immunoprecipitation from *FKBP12.6*$^{+/-}$ cardiomyocyte lysate demonstrating increased PKA phosphorylation of RyR2 at Ser-2808 and *FKBP12.6* depletion after a 30-min exposure to 100 nM isoproterenol (ISO). Pretreatment with 1 μM JTV519 prevented *FKBP12.6* release from RyR2 despite PKA Ser-2808 phosphorylation. (*B*) Bar graphs summarizing results from three myocyte isolations each assessed in triplicate. *P<0.05

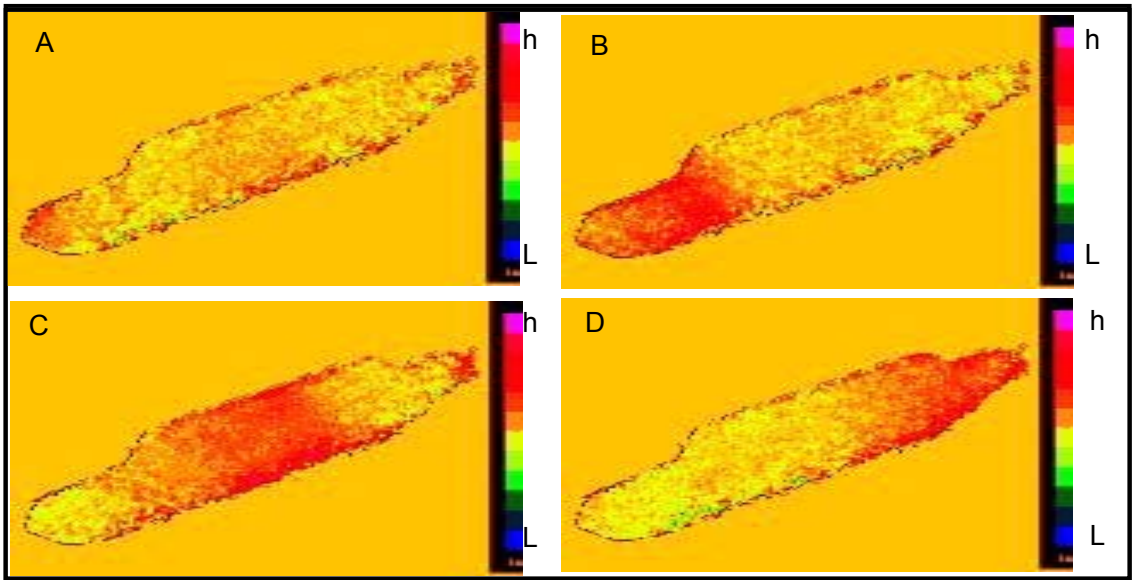

Figure 11 Detection of a sequence of fluorescence ratio metric recordings at rest conditions of a single myocyte after a train of electrical stimuli. The figures show typical spatial profiles of a Ca^{2+} wave. Montages of images corresponding to ~0.1 second, the cell images were captured at 32 msec. interval. Recording of ratio metric images revealed different subcellular calcium propagation. Localized Ca^{2+} signals preceding Ca^{2+} waves characterized by red spots. Ca2+ release propagate at a velocity of – as seen in C and D On the right pseudocolor indicate low (L) and high (h) calcium concentration.

After rapid pacing at 10 s^{-1}, plasma membrane current traces from isolated *FKBP12.6*$^{+/-}$ cardiomyocytes dialyzed with 11 mM EGTA to clamp intracellular $[Ca^{2+}]_i$ at low concentrations showed no I_{TI} before or 4 min after 1 μM ISO treatment (Figure 12*C*). However, *FKBP12.6*$^{+/-}$ cardiomyocytes dialyzed with 1 mM EGTA to clamp $[Ca^{2+}]_i$ at ≈100 nM, which is characteristic for resting cells in diastole, exhibited a low number of I_{TI} events after pacing that were greater than ≈5-fold increased by ISO treatment ($P < 0.05$) (Figure 12*D*). When the identical protocol was repeated in cardiomyocytes pretreated with 1 μM JTV519 and dialyzed with 1 mM EGTA, I_{TI}s were inhibited (Figure 12 *E* and *F*). Thus, either $[Ca^{2+}]_i$ clamp with 11 mM EGTA or JTV519 treatment resulted in significant inhibition of I_{TI}s (Figure 12*F*)

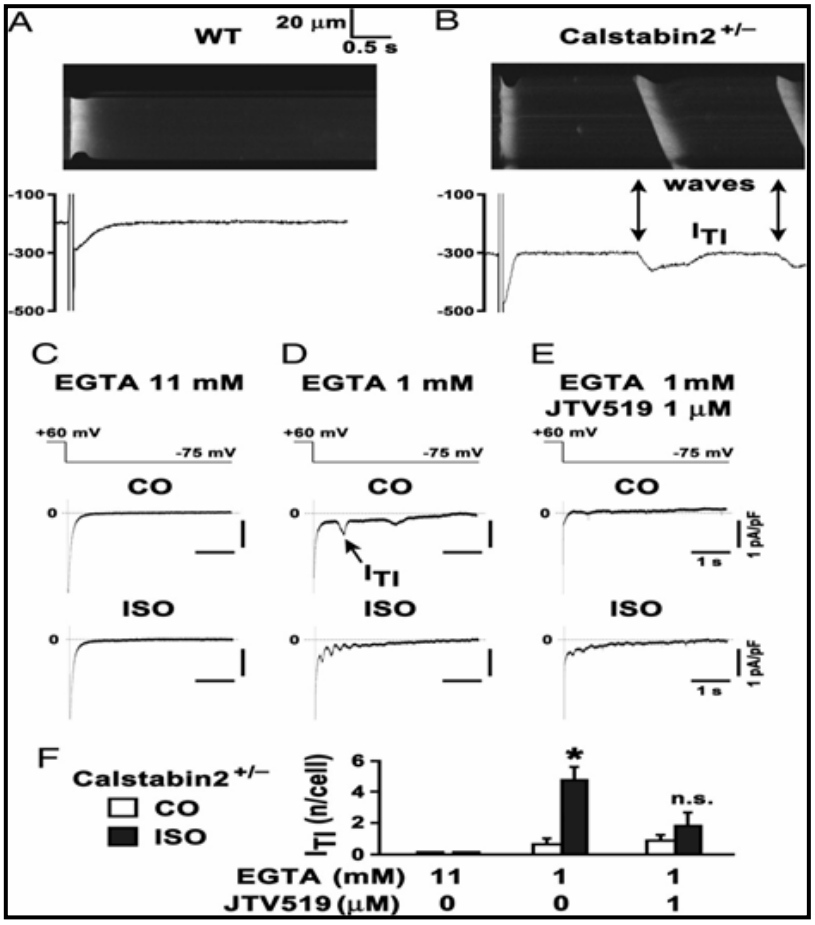

Figure 12. Inhibition of calcium-dependent transient inward current (*I*TI) in haploinsufficient *FKBP12.6*+/− cardiomyocytes by JTV519. (*A*) Confocal Ca^{2+} line scan image of isolated WT cardiomyocyte current trace during 1 μM isoproterenol (ISO). After a depolarization–repolarization step, the *I*Ca tail current rapidly activated a homogeneous intracellular $[Ca^{2+}]_i$ transient followed by a long electrically stable resting phase. (*B*) In contrast, in *FKBP12.6*+/− cardiomyocytes, intracellular Ca^{2+} sparks and Ca^{2+} waves (arrows) were frequent, and Ca^{2+} waves coincide with *I*TI (arrows) under the same conditions. Scales are the same as in *A*. (*C*) Typical current traces were recorded at −75 mV after a preconditioning depolarization train under control conditions (CO) or after 4 min of 1 μM ISO in cells dialyzed with 11 or 1 mM EGTA (*D*) or 1 mM EGTA and 1 μM JTV519 pretreatment (*E*). Scales in *C*–*E* are as indicated. (*F*) Bar graph summarizes average number of *I*TIs per cell under indicated experimental conditions. No *I*TI was detected in cells dialyzed with 11 mM EGTA (*n* = 4, each CO and ISO). In *FKBP12.6*+/− cells dialyzed with 1 mm EGTA, ISO significantly increased the number of *I*TIs per cell (CO, *n* = 6; ISO, *n* = 5; *P* < 0.05). The number of *I*TIs in *FKBP12.6*+/− cells treated with 1 μM JTV519 and dialyzed with 1 mM EGTA was not significantly increased by ISO (CO, *n* = 7; ISO, *n* = 11).

JTV519 mechanism of action and more selective derivates

JTV519 is known to act on multiple targets [16-18] remained possible that the inhibitory effect of JTV519 on AFCs resulted from its impact on Ca^{2+} handling proteins other than RyR2. Thus it was important to assess if JTV519 has any effect on calcium transient. Isolated cardiac myocytes perfused with even low concentration of JTV519 (3μM) shows a marked decrease of intracellular calcium transient (50.61% calcium transient amplitude reduction) (figure 13)

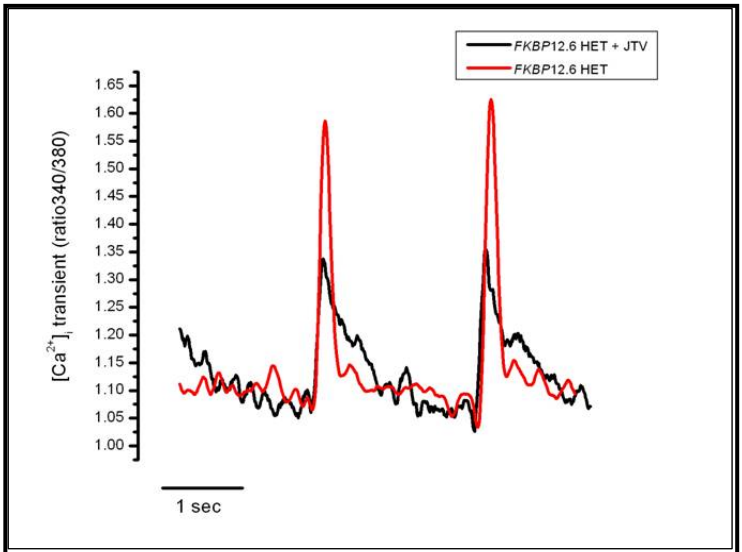

Figure 13. Superimposed calcium transient in Fura-2 electrically stimulated cells (0.5Hz) in red myocytes isolated from an *FKBP12.6* +/- in black the same cell after treatment with JTV519 (3μM for 5 minutes) which clearly reduce the calcium influx.

Calcium flux reduction may reflect the action of JTV519 on the calcium channels. To test this hypothesis we employed whole-cell voltage-clamp technique which allows a quantitative analysis of the JTV519 on cellular ion currents. Results in isolated myocytes (figure 14) shows a significant inhibitory effect of JTV on calcium channel that partially confirm the decreased calcium transient (Figure13).

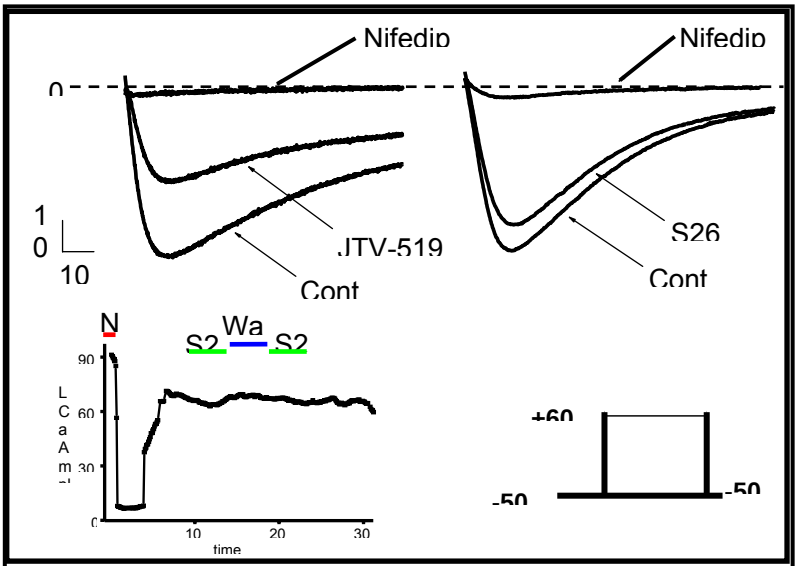

Figure14. Calcium current measured in single ventricular myocytes. Voltage clamped myocytes was injected with step current from a resting potential of -80 mV to +10 mV. The figure show that JTV block calcium current by~50% while a JTV derivate (S26) had only 10% inhibitory effect on the calcium current.

TO increase specificity we biochemically "dissected" JTV519 aiming to isolate the portion of the molecule that interact and associate with RyR2 and cut the portion that has no specific effect. We screened for new JTV519 derivates on isolated myocytes. One compound among many meets the requirement of high affinity for RYR2. We measured the impact of the new compound (that here we call S26 shown in Figure 15) on calcium channel compared to JTV519 using whole-cell patch clamp configuration. The new JTV derivate S26 had a less inhibitory effect of calcium channel, if compared with JTV519 (Figure 14) it remains to be studied if S26 retain the beneficial characteristics we saw in JTV509.

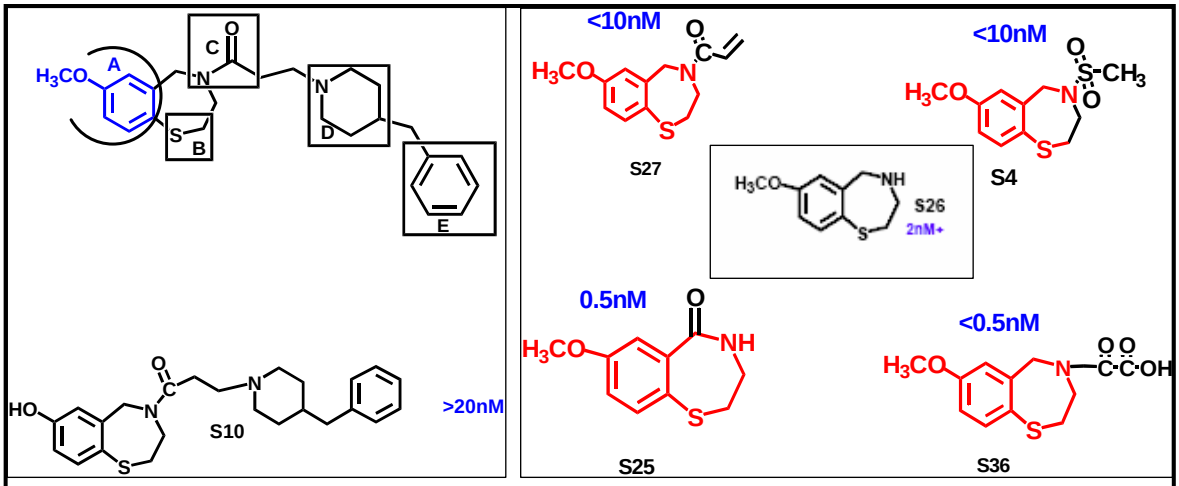

Figure 15 JTV519 molecule structure

Conclusions

In the present study we have shown that *FKBP*12.6 deficiency is associated with aberrant SR Ca^{2+} release, Ca^{2+}-dependent I_{TI}s, MAP alternans, and bidirectional VTs, all of which can be prevented by JTV519 a newly synthesized agent that exert cardioprotective effects.

Our study extends earlier reports showing that intracellular $[Ca^{2+}]_i$ alternans (Figure *9A*) gives rise to action potential alternans at the *in vivo* level. [22,23] We have documented diastolic SR Ca^{2+} leak induced by rapid pacing and β-AR stimulation in *FKBP12.6*$^{+/-}$ mice as a mechanism of MAP alternans and bidirectional VT. Spatially discordant MAP alternans was observed during sustained arrhythmias in *FKBP12.6*$^{+/-}$ mice, suggesting diastolic SR Ca^{2+} leak as a mechanism underlying electrical tissue heterogeneity, as described previously by using optical mapping [20]. SR Ca^{2+} wave fronts in *FKBP12.6*$^{+/-}$ cardiomyocytes consistently activated I_{TI} as a source of electrical membrane instability. In ISO-treated *FKBP12.6*$^{+/-}$ cardiomyocytes, aberrant diastolic SR Ca^{2+} release correlated closely with the pacing frequency (Figure *9C*). Earlier studies showed a relationship between plasma membrane action potential oscillations and $[Ca^{2+}]_i$ alternans. [22,23] Because six distinct CPVT-linked RyR2 mutations exhibited significantly reduced *FKBP*12.6 binding to RyR2 [9,13], *FKBP12.6*$^{+/-}$ cardiomyocytes may represent a model for CPVT. Indeed, the RyR2-R4496C knockin CPVT mouse [24] shows a similar phenotype to that observed in *FKBP12.6*$^{+/-}$ mice, catecholaminergic bidirectional VT. Because the bidirectional VT in the *FKBP12.6*$^{+/-}$ mice was closely associated with MAP alternans throughout the arrhythmia, it seems likely that the alternating bidirectional ECG pattern observed in CPVT is directly related to MAP and $[Ca^{2+}]_i$ alternans. Importantly, enhanced *FKBP*12.6 binding to PKA-phosphorylated RyR2 prevented MAP alternans, I_{TI}s, and

arrhythmias only in *FKBP12.6*$^{+/-}$ mice, further implicating *FKBP*12.6 depletion and diastolic SR Ca^{2+} leak as key antiarrhythmic targets.[19]

Treatment of *FKBP*12.6$^{+/-}$ mice with JTV519 suppressed MAP alternans and cellular I_{TI}s, preventing initiation of ventricular arrhythmias during all pacing protocols. These data indicate that MAP alternans and (as previously shown) DADs in *FKBP12.6*$^{-/-}$ cardiomyocytes [13] may induce propagation of arrhythmic excitation waves. Inhibition of RyR2-mediated diastolic SR Ca^{2+} leak by JTV519 represents a previously unrecognized treatment opportunity for prevention of sudden cardiac death in patients with CPVT and heart failure.

This data suggest that small molecules that increase the affinity of RyR2 for *FKBP12.6* to prevent the Ca^{2+} leaks that trigger arrhythmias could be used to prevent arrhythmia in humans with the same genetic defect, as well as in those suffering from heart failure. Most of the currently available antiarrhythmia drugs have toxic side effects and other therapies—like implanted defibrillators or heart transplants—are expensive and invasive. It would be preferable to take a pill rather than spend hundreds of thousands of dollars on an implant or a heart transplant. New and improved synthesis of JTV519—derived by Columbia Synthetic Organic Chemistry is necessary to eliminate the many non-specific effect of JTV519, the new compounds like the one presented here (S26) needs to be tested to see if the beneficial effect on RyR-2 preventing arrhythmia are retained.

Part II
“The α1D KO mouse model”.

The α1D KO mouse a model for AF

Atria fibrillation is the most common sustained arrhythmia in adult, it is ironic then mechanisms and effective treatments remain incompletely understood and poorly treated. Because no unifying mechanisms of AF have been proven, here we describe the intriguing aspect of a new, recently discovered α1D calcium channel find to be expressed only in the atria. For this goal we used a mouse model where α1D calcium channel was genetically deleted. This will defy the role of the new channel in the atria function, unveil important concept behind current mechanistic theories of AF that will improve our clinical understanding of AF.

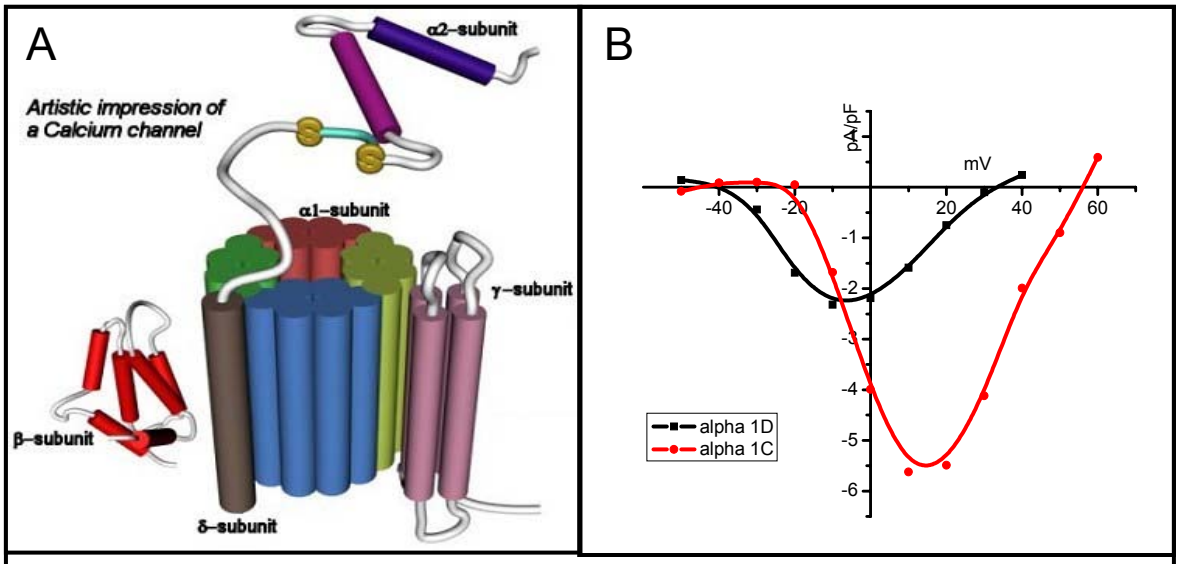

Figure 1. L-Voltage dependent calcium channels A) (L-VDCCs) are heterotetrameric polypeptide complexes comprising. B) Biophysical differences between α1C and α1D in tsA cells.

The L-Voltage dependent calcium channels (L-VDCCs) are heterotetrameric polypeptide complexes comprising the α_1, α_2/δ, ß, and, in some tissues, γsubunits (Figure 1) that allow

depolarization-induced calcium influx into the cytosol. These are considered the functional minimum core for Ca^{2+} channel assembly. The accessory subunits (ß,α_2/δ) are tightly but not covalently bound to the α_1 subunit (Figure 1A) and modulate the biophysical properties and trafficking of the α_1 subunit to the membrane. The Ca^{2+} channel α_1 subunit (170–240 kDa) consists of 4 homologous motifs (I–IV), each composed of 6 membrane-spanning α-helices (termed S1 to S6) linked by variable cytoplasmic loops (linkers) between the S5 and S6 segments (Figure 1A). To date, 10 α_1 subunits genes have been identified and separated into 4 classes: $Ca_v1.1$ (α_{1S}), 1.2 (α_{1C}), 1.3 (α_{1D}), and 1.4 (α_{1F}). The α1D and α1C have different biophysical characteristics. Patched clamp of tsA201 cells transfected with different (α1D and α1C) subunits reveal that α1D has different voltage-current relationship by activating (opening) before α1C does (Figure 1B).

The voltage-gated α_{1D} Ca^{2+} channel was previously considered to be expressed only in neuroendocrine cells [25]. Recent studies reported that the α_{1D} gene deletion in mice leads to sinus bradycardia and various degree of AV-block [26,27]. The evidence presented indicated a critical role of the α_{1D} Ca^{2+} channel in diastolic depolarization and in the rate of discharge in sinoatrial (SA) node cells. The expression of α_{1D} Ca^{2+} channel was demonstrated in the SA-node, AV-node and atria, but not in the ventricles of adult hearts[28-30]. Therefore, abnormalities of α_{1D} Ca^{2+} channel could play an important role in altering the normal activity in the atrium and might also result in arrhythmias, such as atrial fibrillation (AF). A decreased L-type Ca^{2+} current ($I_{Ca\text{-}L}$) density results in a shortening of the action potential (AP) and therefore of the effective refractory period, which occur also in AF [31,32].

A unique property of atrial cells is that both α_{1C} and α_{1D} Ca^{2+} channels contribute to the total $I_{Ca\text{-}L}$[28]. While a decrease in $I_{Ca\text{-}L}$ density, a reduction in mRNA and protein level of the α_{1C} Ca^{2+} channel in AF has been reported [33,34], the role of α_{1D} Ca^{2+} channel in AF remains unclear. One report from a gene microarray study demonstrated a significant reduction in α_{1D} Ca^{2+} channel mRNA (as well as a reduction of α_{1C} Ca^{2+} channel mRNA) in atrial samples from patients with AF [35], supporting an important role of α_{1D} L-type Ca^{2+} channel in the genesis of AF.

However, there are no available pharmacological agents or biophysical approaches to determine the relative contribution of α_{1D} Ca^{2+} channel to the total $I_{Ca\text{-}L}$. The aim of this study was to use the atrial tissues of α_{1D} Ca^{2+} channel deficient mouse (α_{1D} Ca^{2+} channel KO) to investigate the role of α_{1D} Ca^{2+} channel in: (1) the electrocardiographic atrial abnormaliets; (2) the contribution of α_{1D} Ca^{2+} channel to the total $I_{Ca\text{-}L}$; (3) the behavior of the intracellular Ca^{2+} transient; (4) the Ca^{2+} handling by the sarcoplasmic reticulum (SR); and (4) the inducibility of atrial fibrillation (AF).

The results obtained indicate that the elimination of the α_{1D} Ca^{2+} channel results in abnormalities of intracellular calcium homeostasis which in turn affects several electrophysiological functions and facilitate the induction of atrial fibrillation.

Results

Electrocardiograms from mice

Surface ECGs were recorded from a total of 15 α_{1D} KO and 15 WT anesthetized mice. Examples of the ECG recordings are illustrated in Figure 2. The recording from the WT mouse shows a sinus rhythm with regular P-QRS complex and with a detectable P-wave (Figure 2A). The ECG from the α_{1D} KO mice shows sinus bradycardia, and pulses not propagated in the ventricle (A-V block) (Figure 2B, arrow heads). Three out of 15 KO mice showed spontaneous episodes of atrial arrhythmia. The mean QRS-duration was no different in the two groups.

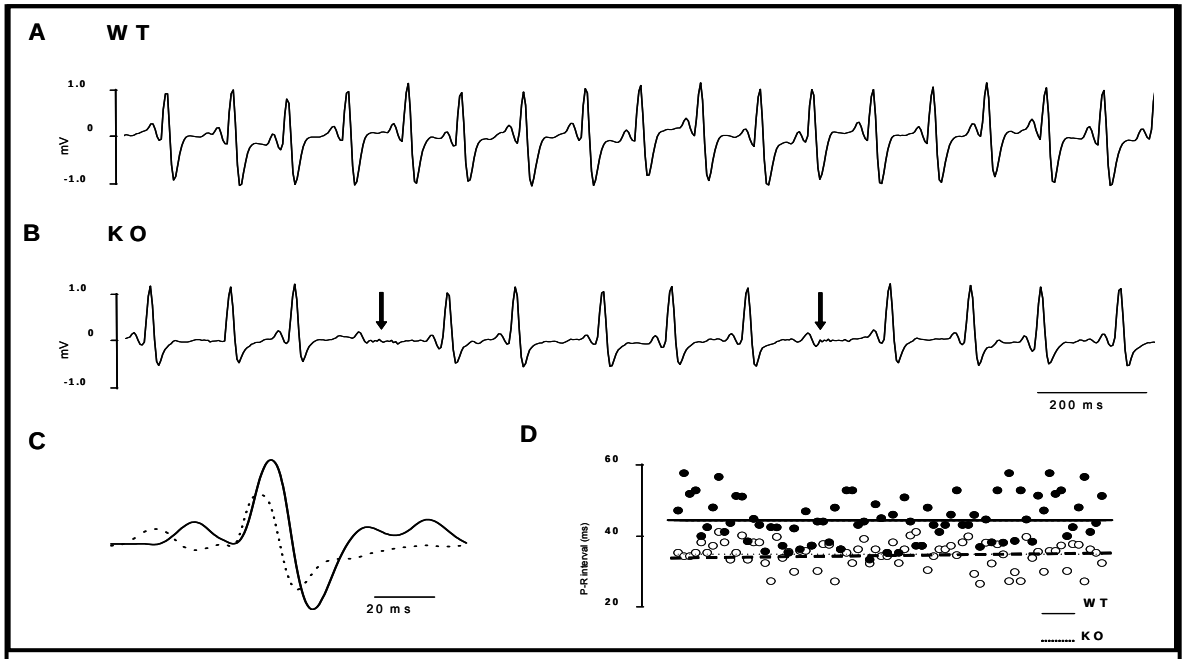

Figure 2. Representative surface ECG recordings from anesthetized mice. (A) ECG showing a sinus rhythm (heart rate of 571 beats/min) with a regular P-QRS complex. **(B)** ECG from an α1D KO mouse with pronounced sinus bradycardia (375 beats/min). AV-block is illustrated by arrow-heads. **(C)** Superimposition of a single P-QRS complex from a WT (solid line) and KO mice (dotted line) shows a prolonged PR-interval. **(D)** Distribution of the P-R interval and average is represented in solid and dotted lines.

Averaged data demonstrated significant sinus bradycardia in the α_{1D} KO mice (551.2 ± 58.5 beats/min in WT *vs*. 303.5 ± 72.4 beats/min in α_{1D} KO mice, $P < 0.01$). In the α_{1D} KO mice the P-wave amplitude was significantly depressed (1.26 $\pm$ 0.06 mV in KO *vs.* 2.24 $\pm$ 0.03 mV in WT mice, $P<0.05$), the P-wave duration was also prolonged (25.3 $\pm$ 1.0 ms in WT mice *vs.* 30.8 $\pm$ 1.0 ms in α_{1D} KO mice, $P<0.05$), P-R interval was also prolonged (33.5 ± 2.02 ms in WT *vs.* 45.07 ± 1.96 ms in the α_{1D} KO mice, $P < 0.05$) (Figs. 2A and 2B). Superimposition of a single P-QRS complex, from a WT and a KO mouse clearly illustrates these differences in the P-wave morphology and the P-R interval between the two groups (Fig. 2A).

Electrocardiograms from isolated hearts and induction of AF in the α_{1D} KO mice

To further explore the cardiac phenotype, we conducted studies in isolated Langendorf-perfused hearts to rule-out interferences from of the autonomic innervations. All the cardiac dysfunctions observed in vivo were still present in isolated the α_{1D} Ca^{2+} channel KO mice hearts (n=5), but not WT mice hearts (n=5), meaning: evidence of SA- and AV-node dysfunctions, sinus bradycardia with an average heart rate of 205 ± 17 beat/min in the α_{1D} Ca^{2+} channel KO heats (n=5) compared with 309 ± 20 beat/min in the WT mice hearts (n=8, $P< 0.01$).

Using the programmed rapid pacing (PRP) protocol, AF was readily inducible in all α_{1D} Ca^{2+} channel KO hearts but in none of the WT mice hearts analyzed. A representative ECG from a WT mouse heart in sinus rhythm is shown in Figure 3A before and after burst stimulation. In contrast, the use of the same burst stimulation protocol resulted in inducible AF/tachycardia in all the α_{1D} Ca^{2+} channel KO mice hearts (5 out of 5) (Figure 3B). Episodes of AF spontaneously converted to sinus rhythm after 125 $\pm$ 66 seconds.

During AF, the atrial rate is clearly faster than the ventricular rate with a median fibrillation interval of ~80 millisecond corresponding to an atrial rate of ~960 beats/minute (Figure 3B).

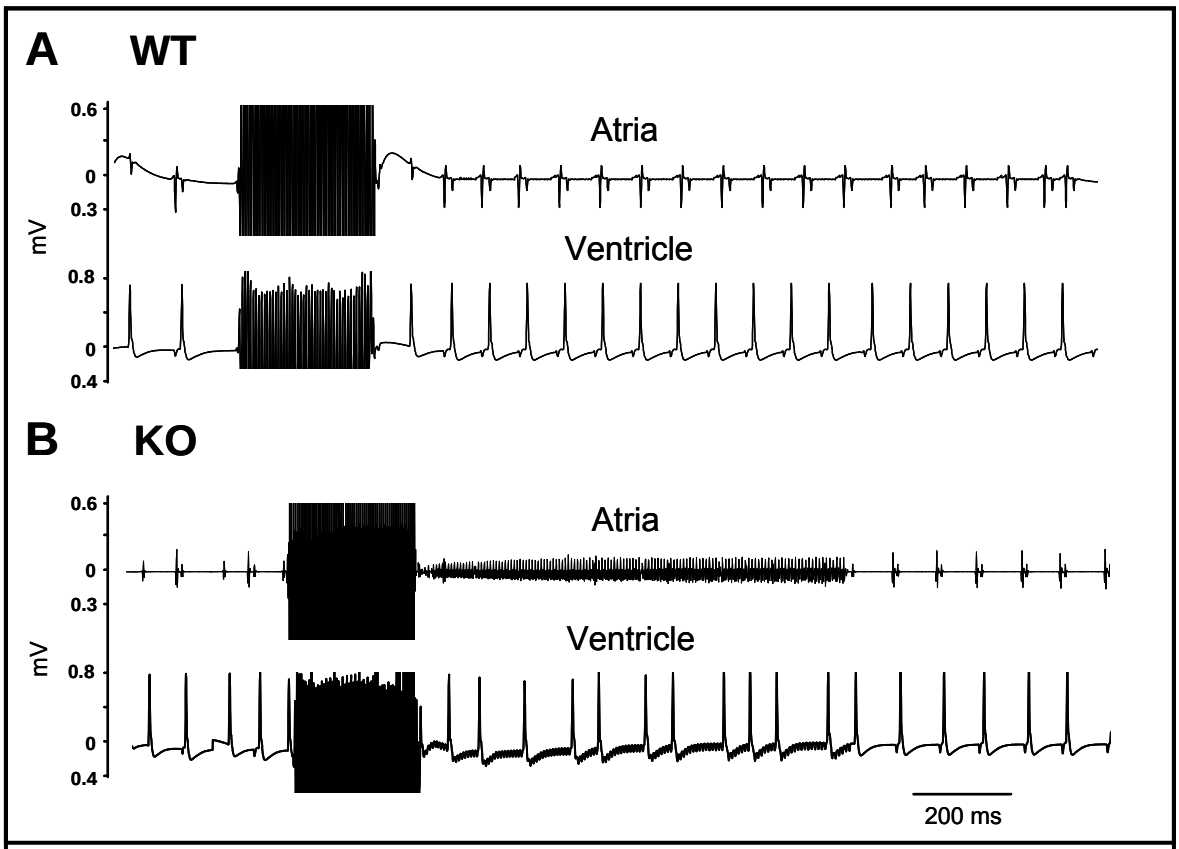

Figure 3. Induction of atrial arrhythmias by rapid pacing in isolated hearts. PRP applied at the S1 cycle length of 40 ms followed by 3 extra-stimuli S1-S2-S3 at 30 ms. (A) Representative epicardial ECG recording from a WT mouse heart, sinus rhythm returned immediately after the burst stimulation. (B) PRP of α1D Ca^{2+} channel KO heart resulted in an episode of AF with slow and irregular ventricular response both of which spontaneously terminated and converted, into sinus rhythm.

Patch Clamp Recordings from Atrial Cells

To determine the relative contribution of the α_{1D} Ca^{2+} channel to the total $I_{Ca\text{-}L}$ in the atrium single cells, RA cells were isolated and the whole cell recording of $I_{Ca\text{-}L}$ was performed. The capacitance of atrial cells from the KO mice cells was slightly but significantly smaller as compared to the WT cells (42.13 $\pm$ 2.22 pF in KO cells *vs.* 50.75 $\pm$ 3.25 in WT cells, n=26 p=0.05). The recording of peak $I_{Ca\text{-}L}$ revealed a positive shift (13 mV) in the KO mice cells as shown in the *I-V* curve (Fig. 4B). Overall atrial myocytes from the KO mice demonstrated a reduced peak of $I_{Ca\text{-}L}$ density as compared with WT (3.51 $\pm$ 0.2 pA/pF in KO mice cells (n=18) *vs.* 4.65 $\pm$ 0.3 pA/pF in WT mice cells (n=25), p<0.05 for WT). The current was normalized with the respective cell capacitance and shown in Figure 4C.

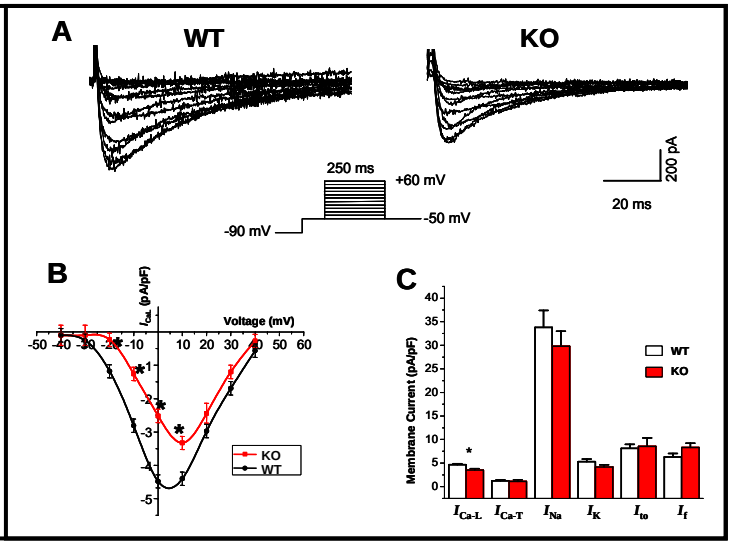

Figure 4. Membrane ion currents in single RA cell from WT and KO mice. (A) Selected *I*Ca-L tracings from WT and KO myocytes. (B) Averaged *I-V* curves shows a reduction of the *I*Ca-L in KO cells (red line) compared with the WT (black line). *I-V* relationship is clearly shifted rightward in KO cells (13 mV). (C) Summary of membrane currents measured in single atrial myocytes. (D) Summary of different membrane current measured in single RA cells. (*P<0.05).

To investigate whether the deletion of α_{1D} Ca^{2+} channel may have resulted in changes (i.e, compensatory mechanisms) of other major atrial ion currents, we recorded I_{Na}, $I_{Ca\text{-}T}$, I_K, I_f and I_{to} from both groups of animals. Current densities between WT and KO mice were not significantly different indicating that deletion of α_{1D} Ca^{2+} channel did not result in

compensation from the currents studied (Figure 4C). To asses the possibility that deletion of α_{1D} Ca^{2+} channel altered the expression of the remaining α_{1C} Ca^{2+} channel, we conducted real-time PCR experiments, (Figure 5) shows that the abundance of mRNA encoding the α_{1C} Ca^{2+} gene is unaltered in α_{1D} KO mice. Thus supporting the idea that the absence of α1D subunit was responsible for the decreased $I_{Ca\text{-}L}$. The transcript for α_{1D} was detected in atria whereas α_{1D} KO mice had none as expected.

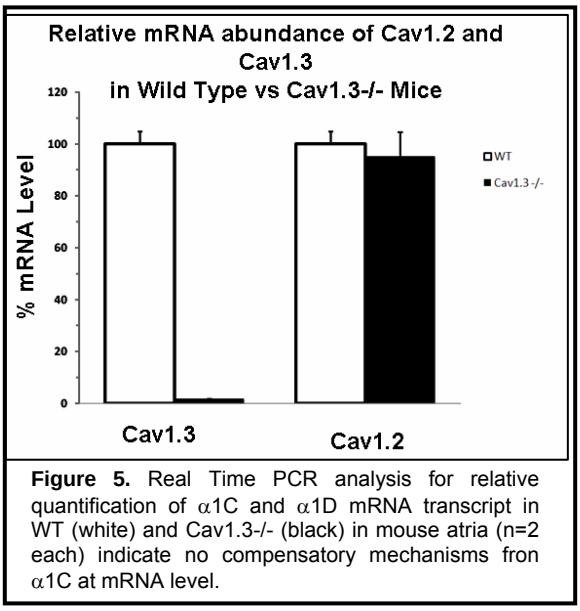

Figure 5. Real Time PCR analysis for relative quantification of α1C and α1D mRNA transcript in WT (white) and Cav1.3-/- (black) in mouse atria (n=2 each) indicate no compensatory mechanisms fron α1C at mRNA level.

Intracellular $[Ca^{2+}]_i$ Measurements in Atrial Myocytes

The $[Ca^{2+}]_i$ transient was monitored in single right atrial cells loaded with fura-2 and electrically field-stimulated. Representative traces of a single atrial cell from a WT and a KO mouse are shown (Figure 6A). A significant reduction of the $[Ca^{2+}]_i$ peck amplitude was observed in all the α_{1D} KO mice atrial cells compared to the WT atrial cells (40.48 $\pm$ 5.02%, n=13, $p<0.05$). Calcium transient reduction was associated with an increase of the time to peak in the KO mice cells without altering the $[Ca^{2+}]_i$ decay time (Figure 6B).

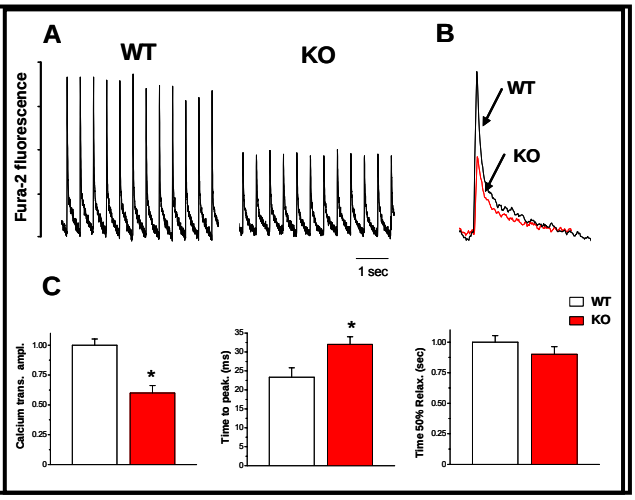

Figure 6. Representative $[Ca^{2+}]_i$ transient from fura-2 loaded cells electrically stimulated at 0.5 Hz. **(A)** $[Ca^{2+}]i$ transient original records from WT and KO atria cells. **(B)** Normalized and superimposed individual $[Ca^{2+}]i$ transient from a WT and from KO show a reduced systolic $[Ca2+]_i$ peak in KO atrial cells. **(C)** Average bar graph showing data for $[Ca^{2+}]_i$ transient amplitude, time to peak, and time to 50% relaxation, (*P<0.05).

SR Ca^{2+} loading and function in the WT and KO mice atrial myocytes

The SR is the main calcium contributor during the calcium transient in mice, we postulated that a decrease in systolic Ca^{2+} might reflect a decrease in SR Ca^{2+} content. To assess our hypothesis we measured SR Ca^{2+} content and the fractional SR Ca^{2+} release. For this purpose, single atrial cells were exposed to rapid caffeine application (10 mM) to empty the intracellular Ca^{2+} store (Fig. 6A). The analysis of the caffeine-induced $[Ca^{2+}]_{iT}$

amplitude reveals a significant reduction of (SR) Ca^{2+} content 17 $\pm$ 2 % (n=8, $p<0.05$) in the α_{1D} KO cells compared with the WT cells.

Fractional release, defined as the fraction (%) of Ca^{2+} release during a transient twitch electrically induced, compared with the total releasable caffeine-induced $[Ca^{2+}]_{iT}$ ($[Ca^{2+}]_{iT}$ twitch/$[Ca^{2+}]_{iT,caffeine}$) was also calculated. The average fractional release in the KO atrial cells decreased significantly (72 $\pm$ 3 %; n=6, $p<0.05$) (Fig. 7C). This result suggests that in the α_{1D} Ca^{2+} channel KO atrial cells the function of the CICR is indeed impaired.

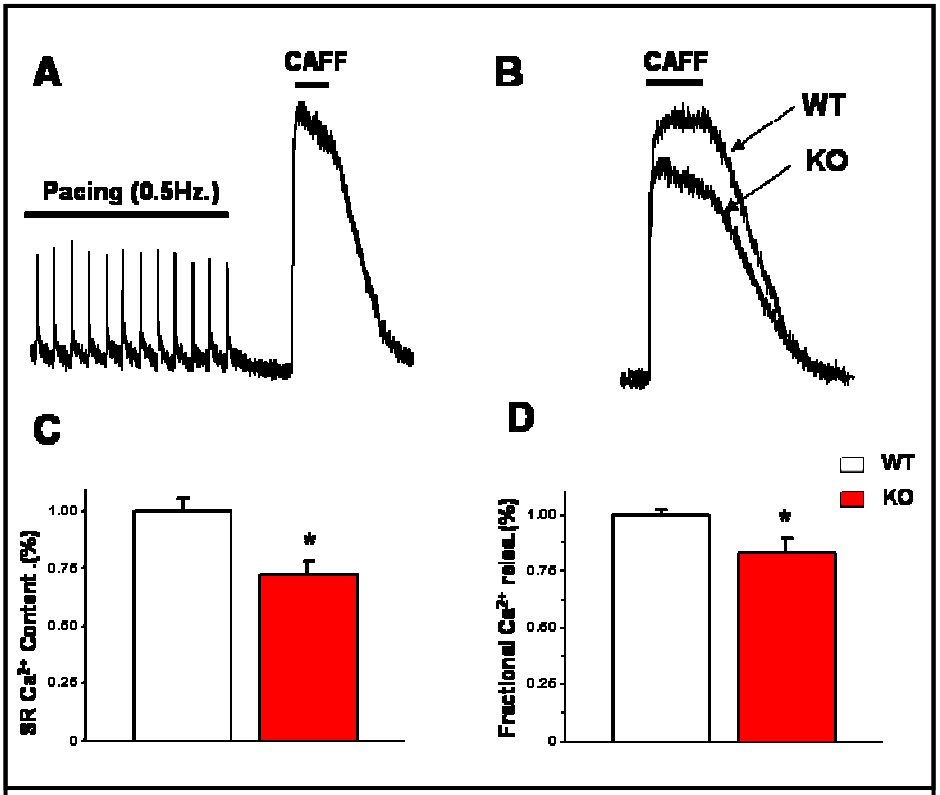

Figure 7. Sarcoplasmic (SR) Ca^{2+} content measured by caffeine application. **(A)** Original traces showing SR Ca^{2+} content measured by caffeine induced calcium release. Cells were electrically field-stimulated followed by caffeine pulse (10 mM). **(B)** Superimposed individual caffeine-induced Ca^{2+} transient from a WT and from a KO cell indicating that the SR Ca^{2+} content in KO cells is less than in WT. **(C)** Average data of caffeine-induced calcium release peak. **(D)** SR fractional calcium released. Data are normalized to facilitate comparison. Data represented

Conclusions

The α_{1D} Ca^{2+} channel is expressed together with the conventional α_{1C} Ca^{2+} channel in the supraventricular tissue of many species [28-30]. The unique role of the α_{1D} Ca^{2+} channel in the heart has been recently emphasized with the generation of α_{1D} Ca^{2+} channel KO mouse. These mice present electrocardiographic abnormalities in absence of any cardiac structural abnormalities.[27] We demonstrate here that α_{1D} Ca^{2+} channel deletion produces cardiac dysfunctions and AF vulnerability. Further we have identified a reduction of $I_{Ca\text{-}L}$ and, abnormal intracellular calcium transient and impaired CICR in the α_{1D} Ca^{2+} channel KO mouse atrial myocytes. These findings may account for the electrocardiographic abnormalities, including AF vulnerability described in these mice.

Electrocardiographic Abnormalities of the α_{1D} Ca^{2+} Channel KO Mice

During ECG recordings in KO mice, spontaneous arrhythmias could be present in addition to sinus bradycardia, P wave changes and first and second degrees AV-block. The smaller and longer P waves suggest a slower impulse atrial propagation in the α_{1D} Ca^{2+} channel KO mouse atria compared to WT. Isolated hearts Langendorff-perfused hearts (which lack the influence of the autonomic innervations) showed the same abnormalities seen in the EGC, indicating that the dysfunctions are likely to be intrinsic in the heart Furthermore, these isolated hearts were prone to AF/tachycardia upon burst stimulation of the right atrium. Although the arrhythmia in intact KO mice does not necessarily have the same mechanism of the AF induced in an isolated heart, the important point is that AF vulnerability of KO mouse is associated (and presumably a consequence) of the α_{1D} Ca^{2+}

channel disruption. Taken all together, the present findings indicate that the α_{1D} Ca^{2+} channel is an obligatory component for the maintenance of normal atrial functions.

Ion Currents in the α_{1D} Ca^{2+} Channel KO Atrial Cells

Reduction of the global RA $I_{Ca\text{-}L}$, which is represented only by α_{1C} in our KO mouse model, indirectly shows that α_{1D} actively contributes to the calcium influx in atrial myocytes for either subsarcolemmal calcium regulation or calcium-induced calcium release (CICR) mechanism. Patch clamp results unmasked the different biophysical characteristics between α_{1C} and α_{1D} channels. The latter activates at more negative potential, consistent with the properties of α_{1D} Ca^{2+} channel characterized in heterologous expression systems.[26,36] That the α_{1C} expression is not altered in α_{1D} Ca^{2+} channel KO mice is indicated by real time PCR results, which show that α_{1C} mRNA is not significantly different in KO mice. Moreover I_{Na}, $I_{Ca\text{-}T}$, I_K, I_f and I_{to} current densities are not affected by the deletion of α_{1D} Ca^{2+} channel in the atrial cells.

These results are consistent with a reduced total $I_{Ca\text{-}L}$ density in the SA node cells of the α_{1D} Ca^{2+} channel KO mice[30] (with no compensatory changes from other currents), but are in contrast with no changes in total $I_{Ca\text{-}L}$ of the α_{1D} Ca^{2+} channel in KO mice atrium.[28] The use of different stimulation/conditioning used to evoke $I_{Ca\text{-}L}$ and differences in the genetic background of the mice used between the two studies[37] may account for the different outcome.

Intracellular $[Ca^{2+}]_i$ transient in the α_{1D} Ca^{2+} Channel KO Atrial Cells

No data are available in the literature regarding the role of α_{1D} Ca^{2+} channel in the calcium transient event in single atrial myocytes. The $I_{Ca\text{-}L}$ reduction in our animal model may account, at least in part, for the significant reduction of the $[Ca^{2+}]_i$ transient in single atrial cells. Since the main source of calcium during CICR is the SR, the smaller $I_{Ca\text{-}L}$ can not be solely responsible for the large calcium transient decrease> in fact, our results show a concomitant SR Ca^{2+} load reduction and a smaller fractional release. The results obtained indicated that α_{1D} Ca^{2+} deletion introduces significant intracellular calcium perturbations that are reflected in abnormal electrophysiological functions. Moreover, reduced calcium channel availability may result in an inefficient CICR.

Pathophysiological Significance

One possible mechanism that explain the cardiac abnormalities in α_{1D} Ca^{2+} channel KO mice is related to the trigger activity of $I_{Ca\text{-}L}$. Because cardiac RYRs are under local control of single L-type Ca^{2+} channels, a change in properties of the L-type channel may have profound consequences on the normal function of CICR. The decrease in L-type channel availability and the positive shift of the *I-V* curve in the α_{1D} Ca^{2+} channel KO mice could be responsible for asynchronous SR Ca^{2+} release that might create microdomains of refractoriness, supporting a critical and unique role of α_{1D} Ca^{2+} channel in the normal and pathological atria. Specifically the present data support the hypothesis that a reduction in $I_{Ca\text{-}L}$ current density may be involved in the initiation of AF, since deletion of this channel makes the mice prone to AF, unlike the reported reduction of $I_{Ca\text{-}L}$ (and I_{to}) current density due to remodeling after AF is in place. The data from present

study contribute information on the characteristic features of the α_{1D} Ca^{2+} channel in the supraventricular tissue which may be useful for the development for potential atrial specific therapeutics targeted towards the management of atrial arrhythmias especially AF.

Methods

Electrocardiographic recordings

Mice were gently removed from their cages and positioned on the ECG recording platform. An array of gel-coated ECG electrodes were embedded in the floor of the platform and spaced to provide contact between the electrodes and animals' paws. the spacing between electrodes was 3 cm, and for nurslings, the spacing was reduced to 2.5 cm. Filter paper, with openings for the electrodes, prevented mouse urine from short-circuiting the signals. The electrodes were connected to an amplifier (MP100 data acquisition system, Biopac). Since even modest handling of mice may induce alterations in heart rate, each mouse was permitted to acclimatize for 10 min prior to collection of baseline data. The signals were digitized with 16-bit precision (Acqknowledge, Biopac) at a sampling rate of 200 samples/second. When mice were sitting or otherwise positioned such that the paws were not in contact with three electrodes, the output from the amplifier was discarded. Only data from continuous recordings of 20-30 ECG signals were used in the analyses. Data were analyzed for heart rhythm, P-wave duration, P-wave amplitude, and QRS duration, first and second heart block.

Epicardial ECG in mouse heart

Hearts were removed and quickly cannulated through the aorta and langendorff-perfused with Krebs-Henseleit buffer containing (mM): 118 NaCl, 4.7 KCl, 1.2 KH_2PO_4, 1.2 $MgSO_4$, 1.8 $CaCl_2$, 25 $NaHCO_3$, and 11.1 glucose, (pH=7.4), bubbled with 95% O_2 - 5% CO_2 at 35 $\pm$ 1 ^oC. Bi-modular amplifier (Biopac. MP system) was used to record independently epicardial ECG from ventricles and atria from a total of 6 chlorinated

electrodes gently placed on the heart. A third module was a stimulator controlled by a computer to deliver programmed fast pacing stimuli with S_1 cycle length ranging from 80 to 40 ms followed by 3 extra-stimuli S_1-S_2-S_3 delivered at a coupling interval of 30 to 20 ms. Stimuli were delivered at the right atrium (RA) at several interval but never more than 1 min continue to induce AF. AF was reordered as spontaneous fast atrial fibrillation not transmitted to the ventricle.

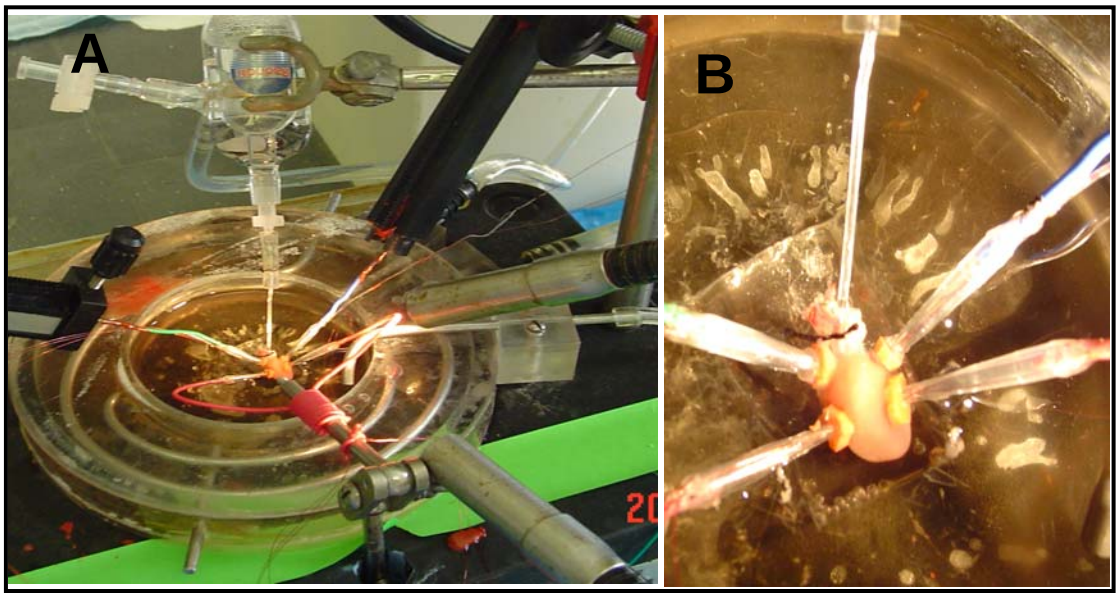

Basic system for heart retrograde perfusion mode (Langendorff) for stimulation and epicardial ECG recordings.

ECG analysis

Each signal was analyzed using Acqknowledge (Biopac) software specialized in physiologic waveform analysis. Digital filtering of frequencies below 2 Hz and above 100 Hz was applied to minimize environmental signal disturbances. The software uses a peak detection algorithm to find the peak of the R-waves and to calculate heart rate. Heart rate variability was calculated as the mean of the differences between sequential heart rates for

the complete set of ECG signals. The T-wave is not separate from the QRS in rodent ECG`s. We defined the end of the T-wave of each signal as the point where the signal returned to the isoelectric line. The mean voltage between the preceding P-wave and QRS interval.

Removal of the heart

After inducing anesthesia with halothane or isofluorane (4-2% mixed with oxygen), the mouse was placed in a dissecting tray near the isolated heart apparatus. To facilitate fast removal and mounting of the organ, extra sets of sutures and instruments was positioned close at hand. Cardiac removal was performed as a surgical procedure, after exposing the heart by a sternotomy cutting and retracting the rib cage, two loose ties are placed around the aorta. One tie is used to manipulate the aorta and the other to secure the aorta to the cannula (custom made plastic cannula). An extension catheter with perfusate solution is placed on the cannula for ease of preparation. This cannula can be connected to the perfusion apparatus and a slow stream of perfusate is permitted to flow through the aortic cannula, air bubbles must be absent since their will not allow complete and homogeneity during heart perfusion. The pulmonary artery is then cut, followed by a partial cut across the aorta. The cannula is then inserted and secured with the ties. The tip of the aortic cannula should not be inserted below the base of the aorta, as the ostium may be occluded (coronary perfusion restricted) or the aortic valve may be damaged. Once perfusion has commenced, the heart may be removed from the animal and the cannula disconnected from the extension tube and placed in the apparatus. As the heart is a highly metabolically active organ, it requires a constant supply of oxygen and nutrients. Therefore, the time in which it takes to remove and mount the heart is very important. An extended period (> 30

seconds) of reduced oxygen and/or nutrients will significantly affect cardiac tissue (at body temperature), in particular its survival and experimental responses.

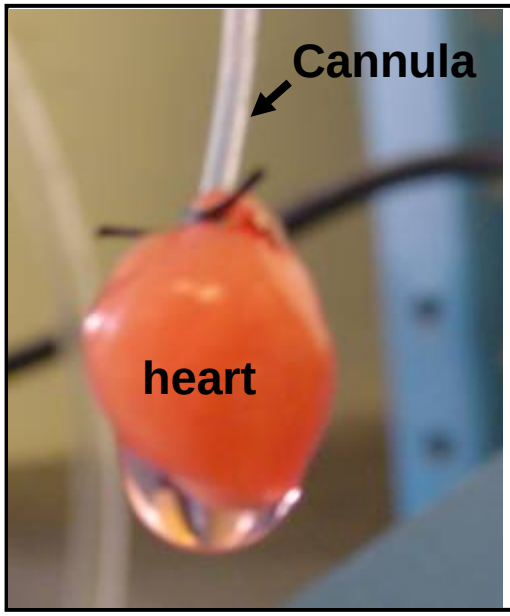

Mouse langendorff preparation consists of a retrograde system which perfuses the coronary vascular system of an isolated heart via the aorta through a cannula with oxygenated fluid (such as Krebs-Henseleit) from a reservoir to study coronary flow during cardiac activity. Models are maintained at constant mean flow (using an in-line flowprobe inserted into the perfusion line).

Epicardial ECG in mouse heart

Hearts were removed and quickly cannulated through the aorta and langendorff-perfused with Krebs-Henseleit buffer containing (mM): 118 NaCl, 4.7 KCl, 1.2 KH_2PO_4, 1.2 $MgSO_4$, 1.8 $CaCl_2$, 25 $NaHCO_3$, and 11.1 glucose, (pH=7.4), bubbled with 95% O_2 - 5% CO_2 at 35 $\pm$ 1 ^{o}C. Bi-modular amplifier (Biopac. MP system) was used to record independently epicardial ECG from ventricles and atria from a total of 6 chlorinated electrodes gently placed on the heart. A third module was a stimulator controlled by a computer to deliver fast pacing stimuli with S_1 cycle length ranging from 80 to 40 ms followed by 3 extra-stimuli S_1-S_2-S_3 delivered at a coupling interval of 30 to 20 ms. Stimuli were delivered at the right atrium (RA) at several interval but never more than 1

min continue to induce AF. AF was recorganized by spontaneous fast atrial fibrillation with a typical saw tooth configuration not completely transmitted to the ventricle.

Isolation of mouse ventricular myocytes.

Cardiomyocytes from WT, *calstabin-2*+/-, or *calstabin- 2*-/- mice were enzymatically dissociated and isolated as described:

Dissection:

1. Inject heparin 0.25 ml/mouse (5000 U/I)
2. After at least 30 min inject (xylazine 20 mg kg-1 plus ketamine 100 mg kg-1) an alternative could be anesthesia with isofluorane/ halothane 4% inductance, 1.5 % maintenance + 100% oxygen. Open the thorax by serotomy and the heart was quickly excised and cannulated at the bottom of a Langendorf perfusion system. Wash for 5 min with Basic Buffer/tyrode solution* Ca^{2+}- free at constant volume 3ml/min.
3. Change the perfusion solution to Digestion Solution (Perfusion solution + 20 mg collagenase. Type II act 275 + 5 mg protease. Type XIV + Hyaluronidase).
4. Place the heart in a clean dish with Digestion Buffer, remove the right ventricle and the supraventricular tissue, and after mechanic agitation transfer the cell and tissue in a 15 ml tube add 0.5% serum FCS or BSA to inactivate the enzymes.
5. Remove the supernatant, wash 3 times with Ca^{2+} restore solution (I-II-III).
6. Finally resuspend in Tyrode solution (1.2 mM Ca^{2+}).

(All the solution must be pre-warmed before use)

Solution for single myocytes isolation and culture

Basic Buffer. 1000 ml pH 7.4

COMPOUND	CODE	QUANTITY	
MEM	SIGMA	M-0518	1 BOTTLE
HEPES	SIGMA	H-3375	0.7 gr
L-GLUTAMINE	SIGMA	G-7029	0.3 gr
TAURINE	SIGMA	T-0625	1.25 gr
INSULINE*	SIGMA	I-5500	20 U (ITSSMS,
I-1884 10 ML)*			
ANTIBIOTIC*	SIGMA	P-3539	10 ml*
H_2O DISTILLED			

You can add BDM sigma B-0753 10 μM for adult 1 μM for neonatal.

- only for cell culture.

Incubation Buffer. 50ml pH 7.4

I.B. mL	100	300	500
Basic Baffer + B.S.A. gr (0.5%)	0.5	1.5	2.5

Albumin Sigma A-4503 or fraction IV Sigma 2153. Check the pH 7.4, filter (for cell culture) before use.

Digestion Buffer.

Basic Buffer	50 ml
Collagenase type II	Activity 317 worthington 20 mg/ml for 18-20 min for adult mouse + 0.15 mg Protease XIV (sigma).

$CaCl_2$ Stock solution (10 mM) in 10 ml of Tyrode or basic buffer

Final conc.

(I) 2.5 ul 25 uMol

(II) 10 ul 0.1 mmol

(III) 50.0 ul 0.5 mmol

Tyrode solution pH 7.4 (1 liter)

120 NaCl	8.4 gr
5.4 KCl	0.402
5 MgSO4	1.0 ml
20 glucose	1.8 gr
10 HEPES	2.2 gr

Add $CaCl_2$ pH 7.4, pre-oxygenated with 100% O2 for 5 min.

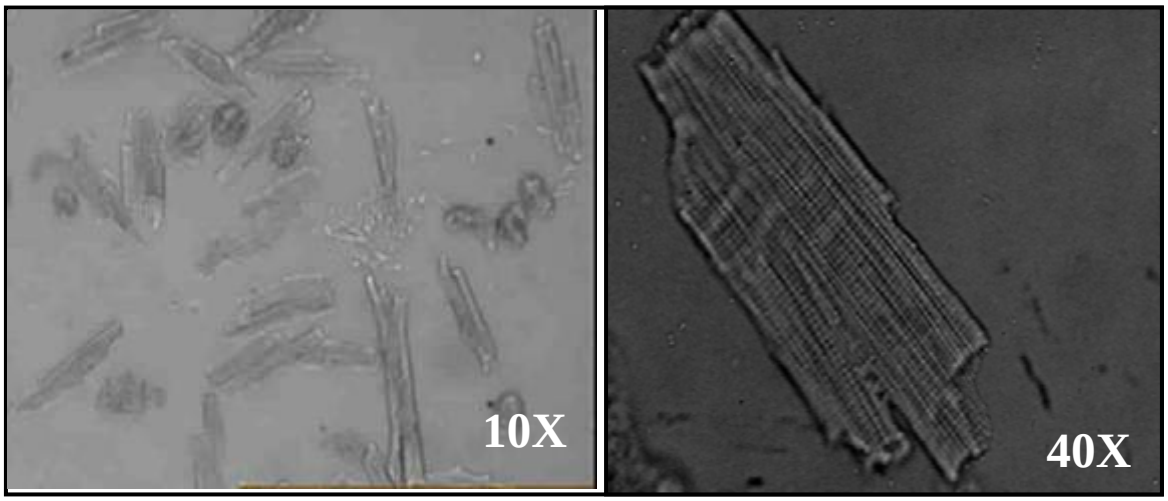

Enzymatically isolated calcium tolerant cardiomyocytes from mouse left ventricle at 2 different magnifications.

Isolation of mouse atrial myocytes

Atrial cells were isolated from Langendorff-perfused hearts. The heart was perfused with nominally Ca^{2+}-free Tyrode's solution containing (mM): 137 NaCl, 5.4 KCl, 1 $MgCl_2$,

0.33 NaH_2PO_4, 10 HEPES and 10 glucose (pH=7.4) equilibrated with 100% O_2 (35 $\pm$ 1 ^oC). After the blood was washed out. Digestion beging with 5 minutes digestion wit DNAsa and trypsin (0.5 and 1 mg/ml respectively). After the heart was perfused with

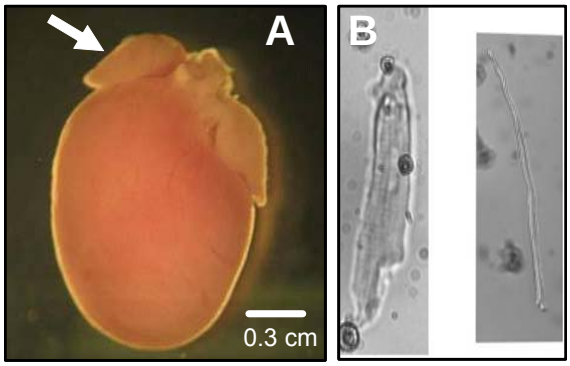

In A) Isolated mice heart, the right atrium is indicated by the white arrow in B) cells isolated from the right atrium at 40X, note the different morphology

perfusion solution containing: collagenase type-2 (1 mg/mL, Worthington, Biochemical Corp.), protease type XIV (0.02 mg/mL; Sigma), and elastase (0.2 mg/mL, Worthington, Biochemical Corp.). When the hearts became swollen, the right atrium was quickly removed and the tissue was allowed to digest for an additional 5-15 minutes in the solution containing the enzymes. Never agitate or add bsa prior to cell separation The tissue was than transferred into the KB-recovery solution and cells were dispersed after 40 minutes of incubation. Na^+ and Ca^{2+} were re-introduced by the addition of a solution containing (mM): 10 NaCl, 1.8 $CaCl_2$, and BSA (1mg/mL). Cells were finally stored in a solution containing (mM): 100 NaCl, 35 KCl, 1.3 $CaCl_2$, 0.7 $MgCl_2$, 14 L-glutamic acid, β-OH butyric acid, 2 KH_2PO_4, 2 taurine and BSA 1 mg/ml, (pH=7.4) and were used within 4 hours after the isolation.

Intracellular Ca^{2+} measurement and imaging in isolated ventricle myocytes.

Calcium indicator - Fura-2

The most widely used method of Ca^{2+} monitoring is by the use of fluorescent Ca^{2+} indicators, a technique pioneered by professor Roger Tsien and colleagues (Tsien, R. in *Methods in Cell Biology,* Vol. 30, Taylor, D.L. and Wang, Y-L, Eds., Academic Press (1989) pp. 127-156). These indicators probe Ca^{2+} concentration via their fluorescent spectral changes upon Ca^{2+} binding. These products are available in both the membrane-impermeant salt forms and the membrane-permeant AM ester forms. The AM esters of the indicators are membrane-permeant and thus can be loaded into cells by simple incubation of the cell or tissue preparation in a buffer containing the AM ester. Pluronic F-127, a mild nonionic detergent that can facilitate the loading of the AM esters must be present during the incubation. The AM esters themselves do not bind Ca^{2+} . However, once they have entered the cells, they are readily hydrolyzed by intracellular esterases into the parent Ca2+ indicators, thus becoming responsive to Ca^{2+}.

One of the widely used is Fura-2 a UV-excitable fluorescent calcium indicator. Upon calcium binding, the fluorescent excitation maximum of the indicator undergoes a blue shift from 363 nm (Ca^{2+}-free) to 335 nm (Ca^{2+}-saturated), while the fluorescence emission maximum is relatively unchanged at ~510 nm. Measurement of the bound/unbound Fura-2 emission light from a single cell is an indirect measurement of the amount of calcium within that cell citoplasmatic calcium content. Fura-2 is typically excited at 340 nm and 380 nm respectively and the ratio of the fluorescent intensities corresponding to the two excitations is used in calculating the intracellular concentrations. Measurement of calcium concentration using this rationing method avoids interference due to uneven dye

distribution and photobleaching (Bright, G.R., et al, in Fluorescence Microscopy of Living Cells in Culture, Part B, (Methods in Cell Biology, Vol. 30), Academic Press (1989) p. 157). Fura-2 has been used in many cellular systems and applications, particularly in microscopic imaging as well all the experiments in this thesis.

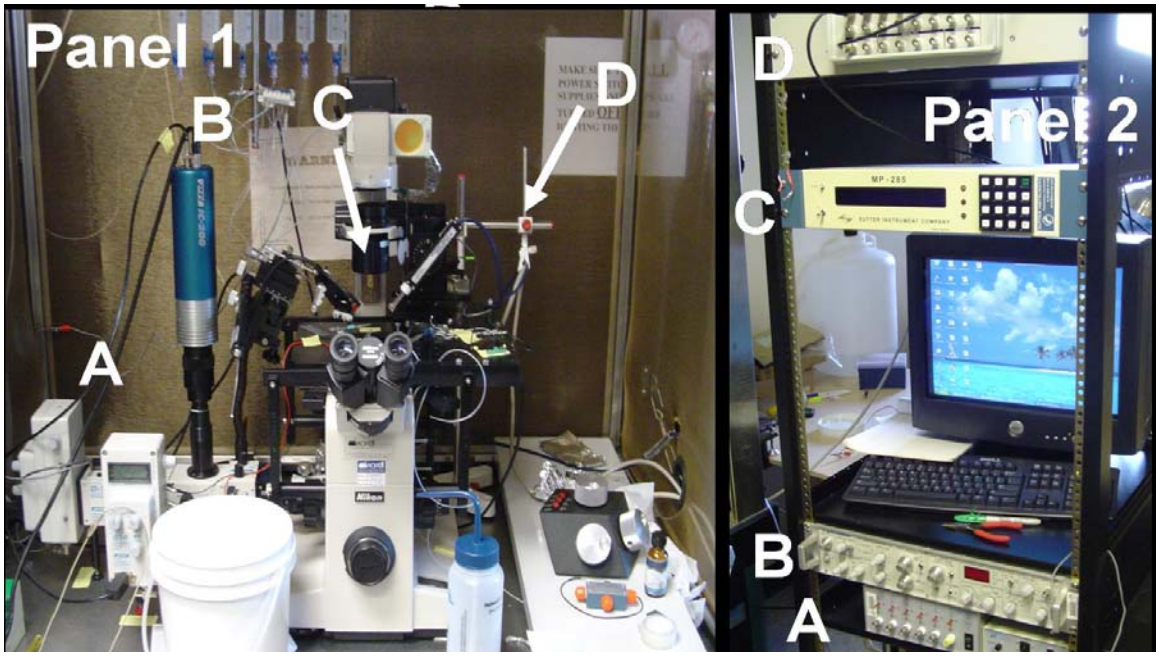

System I set up for fluorescence, imaging and ion channel activity in living cells. Panel 1: A) Fluorescence detectors for emission shifted dyes. B) Intensified CCD camera. C) Microperfusion system. D) Microelectrode holder for patch. E) Micromanipulator. Computer patch clamp set-up. Panel 2: A) Microperfusion controller. B) Amplifier. C) Micromanipulator controller. D) Digitizer

Calcium transient measurement

Ventricular or atria single cells were incubated in a 10 μM solution of fura-2 AM acetoxymethylester ester (Invitrogen) (3 μM in case of the atria cells) dissolved in DMSO in presence of pluronic F-127 (5 μl/ml) 30 min at room temperature, followed by resuspension in fura-2-free solution for 30 min to allow de-esterification. Cells were plated in a perfusion chamber placed on the stage of an inverted microscope (Nikon) coupled to a video camera. Cell length was monitored with a video-edge detector. For $[Ca^{2+}]_i$ measurements, fura-2 fluorescence was measured by using a photomultiplier (DeltaRam; PTI, South Brunswick, NJ). The ratio of emitted fluorescence at 340 and 380 nm was converted to $[Ca^{2+}]_i$ units. Cardiomyocytes were field-stimulated with 3-ms pulses at increasing frequencies (0.5–8 s^{-1}) by programmed field stimulation (ALA Scientific Instruments, Westbury, NY) in the presence of 100 nM ISO at 37°C. Some cells were pretreated with 1 μM JTV519 or the carrier solution (0.1% DMSO) for 2 h.

As for measurements ventricular myocytes were viewed with a 40 oil-immersion objective (Fluor, N.A. 1.3, Nikon) and loaded with the dye and excited (PTI Delta ram system) at 72 W intensity on the cell. The fluorescence was detected at 515 $\pm$ 15 nm with an photomultiplier (PTI) operated by an algorithm in the photon counting mode. The recording chamber was connected to a barrel to ensure continues superfusion of the cell (200 μl volume) stimulator electrodes were at the extremes and the bottom was thin glass (0.01 mm).The acquiring velocity was set to 100 points per second.

Amplitude, time course and Ca^{2+} concentration was calculated from fluorescence images using an established self-ratio calibration procedure. Graph plots were generated from Felix (PTI software and Origin).

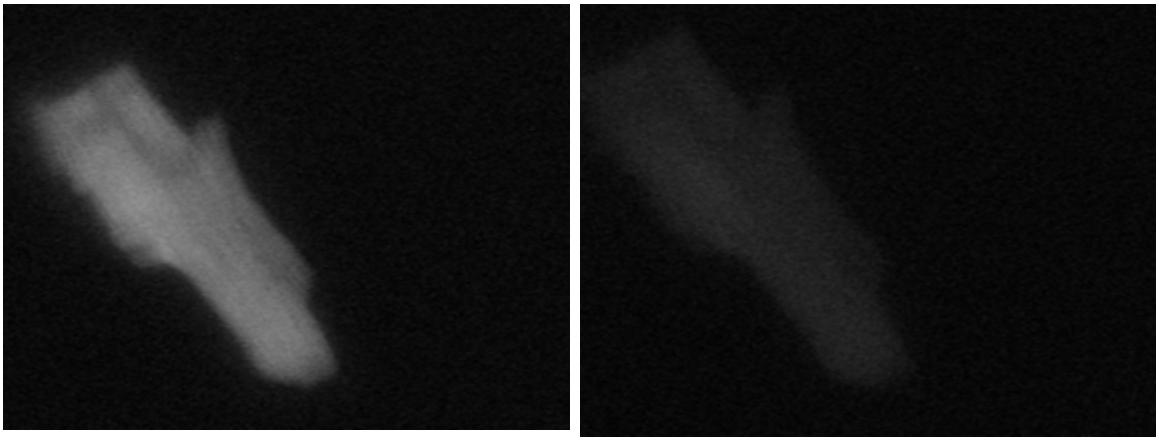

Figure Isolated ventricular myocytes loaded with fluorescent dye and UV-excited (indo-1 in this case)

SR Ca^{2+} loading measurement

Caffeine was applied in a solution of the following composition: (in mM) 10 caffeine, 140 LiCl, 4 KCl, 10 glucose, 5 HEPES, 1 $MgCl_2$, 4 4-aminopyridine. Caffeine was used to release SR Ca^{2+} content and thus estimate SR Ca^{2+} loading after a period of pacing (0.5 Hz). Na^+ and Ca^{2+} were not included in the caffeine solution to minimize extrusion of Ca^{2+} by the Na^+/Ca^{2+} exchanger. Caffeine was applied by pressure-ejection through a pipette positioned near the cell (200 μmeter) that empties the SR Ca^{2+} store after cells were electrically stimulated at steady state.

Confocal Ca^{2+} measurements

For imaging studies ventricular myocytes were viewed with a 40 oil-immersion objective (Fluor, N.A. 1.3, Nikon) and loaded with Fluo-4 was excited with the 488 nm line of an Mercury lamp (PTI Delta ram system) at 72 W intensity on the cell. The fluorescence was detected at 515 $\pm$ 15 nm with an intensified camera (PMT IC. 300) operated by an

algorithm in the photon counting mode. The recording chamber was connected to a barrel to ensure continues superfusion of the cell (200 μl volume) stimulator electrodes were at the extremes and the bottom was thin glass (0.01 mm).The acquiring velocity was set to 100 points per second. Amplitude and time course of Ca^{2+} signals due to Ca^{2+} influx were computed off-line using a the NIH Image software (NIH, Bethesda,MD). The spatial profiles of $[Ca^{2+}]_i$ are limited by optical diffraction. Ca^{2+} concentration was calculated from fluorescence images using an established self-ratio calibration procedure (Cheng et al., 1993). Surface plots were generated from Felix (PTI software and Origin).

Gene expression analysis for α1C and α1D transcripts using real time PCR

Total cellular RNA was isolated from atrial tissue of WT and α1D KO mice (n=2 each) using Trizol LS Reagent (Invitrogen) according to the manufacturer's recommendations. RNA was quantified by spectrophotometry at 260 nm and the ratio of absorbance at 260 nm to that of 280 nm was > 1.8 for all samples. Degradation of RNA was monitored by the observation of appropriate 28S to 18S ribosomal RNA ratios as determined by ethidium bromide staining of agarose gels. First strand cDNA synthesis was carried out using RETROscript reverse transcriptase kit (Ambion). Gene specific Taqman primers (Applied Biosystems) were used to quantify the relative changes in mRNA levels of α1C and α1D in WT and α1D KO mice using ABI PRISM 7500 Real Time PCR (Applied Biosystems). All Real-Time PCR reactions were done in triplicates and the C_T values normalized against the endogenous control 18S.

Simultaneous Recording of I_{TI}s and Confocal Imaging of Ca^{2+} Sparks and Ca^{2+} Waves

To simultaneously measure I_{Ca}-induced Ca^{2+} release from the SR, fluo-4 was excited at 488 nm, and the fluorescence was detected at 510 nm with a laser scanning confocal microscope (LSM 510; Zeiss). Cell capacitance and I_{Ca} density were calculated with CLAMPEX 9.0 (Axon Instruments). Global Ca^{2+} release was analyzed by routines compiled with IDL 6.0 (Research Systems, Boulder, CO). Myocytes were incubated with fluo-4 acetoxymethylester (10 μM) and, after a 20-min period, were superfused with an extracellular solution containing 1.8 mM Ca^{2+}. Cells were field-stimulated at 1.0 Hz to produce steady-state conditions. Within the first 10 s after the last depolarization of a 15-pulse train, spontaneous non propagating Ca^{2+} release was recorded for the next three to four image frames at high resolution (800 lines per frame, 1.92 ms per line) and identified as "diastolic Ca^{2+} sparks." The recording sequence was repeated three times in each cell. Line-scan images were analyzed and Ca^{2+} sparks were detected offline with a computer-based detection algorithm.

In vivo electrical mapping

Subcutaneous six-lead ECG recordings were obtained (model VR12; Electronics for Medicine, Pleasantville, NY). An MAP contact electrode was gently placed on the left ventricular anterior free wall by using a 3D micromanipulator and digitized MAP recording was used to monitor changes in epicardial membrane potential. A small platinum electrode was placed on the right ventricular free wall for PES. Pacing (S1–S2) at CLs between 70 and 200 ms, interpolating a single premature stimulus every 10 beats, was performed to determine effective refractory period at twice diastolic threshold

strength. Rapid pacing was increased until 2:1 block. In a subset of mice, two MAP electrodes were gently placed on the left anterior free wall during sustained VTs. Animals were treated with either JTV519 (7-day continuous infusion 0.5 $mg \cdot kg^{-1} \cdot hr^{-1}$) or placebo (carrier). ISO was administered by i.p. injection (0.5 $mg \cdot kg^{-1}$) [19]. CL was averaged from 10 consecutive RR intervals.

Transfection of tsA201 cell line

The mammalian cell line tsA201 is derived from human embryonic kidney HEK-293 cells by stable transfection with SV40 large-T antigen. Cells were grown in high-glucose DMEM supplemented with 10% fetal bovine serum, L-glutamine (2 mM), penicillin G (100 U/ml), and streptomycin (10 mg/ml; GIBCO BRL Life Technologies). Cells were incubated in a 5% CO_2 humidified atmosphere. The tsA201 cells were transfected using the Ca^{2+} phosphate method with the following modification: to identify transfected cells, 7 μg of EBO/CD8 plasmid was cotransfected with 7 μg of each of α_{1D}, β2a and α2δ cDNAs. Transfected cells that bind beads generally also express Ca^{2+} channels. For patch-clamp experiments, cells 2–3 days posttransfection were incubated for 2 min in medium containing anti-CD8-a coated beads (M-450 CD8-a; Dynabeads). The unattached beads were removed by washing with extracellular solution. Beads were prepared according to the manufacturer's instructions (Dynal Biotech, Brown Beer, WI). Cells expressing CD8-a, and therefore binding beads, were distinguished from nontransfected cells by light microscopy.

Patch clamp technique

Patch clamp traditionally uses a glass pipette, with an open tip diameter of about one micrometer, and is made such that the tip forms a smooth surfaced circle, rather than a sharp point. This style of electrode is known as a "patch clamp electrode" and is distinct from the "sharp microelectrode" used to impale cells in traditional intracellular recordings. The interior of the pipette is filled with different solutions (usually called the pipette solution) depending on the specific technique or variation used (see following). For example, with whole cell recordings, a solution that approximates the intracellular fluid is used. A metal electrode in contact with this solution conducts the electrical changes to a voltage clamp amplifier. The researcher can change the composition of this solution or add drugs to study the ion channels under different conditions. The patch clamp electrode is pressed against a cell membrane and suction is applied to the inside of the electrode to pull the cell's membrane inside the tip of the electrode. The suction causes the cell to form a tight seal with the electrode (a so-called "gigaohm seal", since the electrical resistance of that seal is in excess of a gigaohm). Unlike traditional voltage clamp recordings, the patch clamp recording uses a single electrode to voltage clamp a cell. This allows a researcher to keep the voltage constant while observing changes in current. Alternately, the cell can be current clamped, keeping current constant while observing changes in membrane voltage.

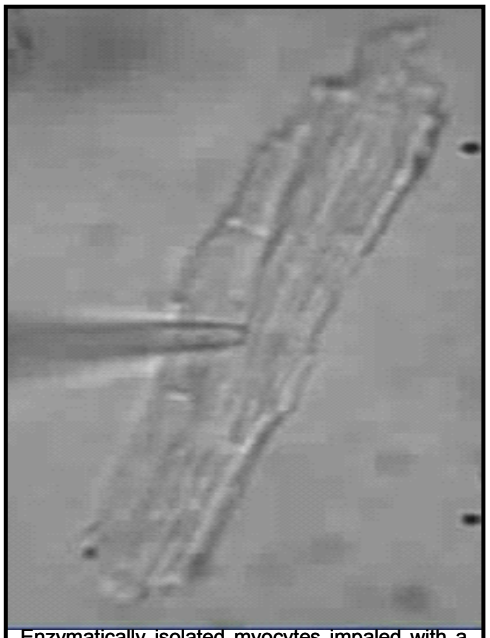

Enzymatically isolated myocytes impaled with a patch clamp pipette (whole-cell configuration)

Recording of α_{1D} $I_{Ca\text{-}L}$ in tsA201 cells.

Whole cell voltage-clamp recording was performed with the Axopatch 200B (Axon Instruments) with recording patch pipettes resistance of 1.5–2 MΩ. The internal solution contained (in mM) 135 CsCl, 4 $MgCl_2$, 4 ATP, 10 HEPES, 10 EGTA, and 1 EDTA; adjusted to pH 7.2 with tetraethylammonium (TEA)-OH. The bath solution contains (in mM) 135 choline Cl, 1 $MgCl_2$, 2 $CaCl_2$, and 10 HEPES; adjusted to pH 7.4 with TEA-OH. Signals were sampled at 20 kHz and low pass filtered at 2 kHz. Data were leak subtracted on-line using the P/4 protocol and analyzed using pCLAMP V8.0 (Axon Instruments). Junction potentials were always compensated and were <5 mV. For α_{1D} $I_{Ca\text{-}L}$ current-voltage relations, tsA201 cells were depolarized from a holding potential of –100 mV to test potentials between –80 and 60 mV with increments of 10 mV. For the time course, α_{1D} $I_{Ca\text{-}L}$ was continuously recorded at a test potential of –10 mV from a holding potential of –100 mV.

Whole-cell recording of ionic currents in atrial cells

Whole-cell voltage-clamp was used for current recordings. Cells were first superfused with Tyrode's solution, then the perfusion was switched to the appropriate solution for each current studied. Experiment were conducted at room temperature, briefly, for $I_{Ca\text{-}L}$ and $I_{Ca\text{-}T}$, Na^+ and K^+ were substituted by equimolar concentration of tetraethylammonium (TEA^-) and Cs^+ respectively. Niflumic acid (30 μM), and 4-aminopyridine (4-AP, 1 mM), were added to block chloride and K^+ outwards currents; cobalt (5mM) was added during $I_{Ca\text{-}T}$ recording. The pipette solution used for $I_{Ca\text{-}L}$ and $I_{Ca\text{-}T}$ was similar, and contained (mM): 110 Cs-aspartate, 20 CsCl, 1 $MgCl_2$, 10 EGTA, 10 HEPES, 5 Mg-ATP and 0.5 tris-GTP, pH 7.4 with CsOH. The $I_{Ca\text{-}L}$ was activated by a series of 200-ms depolarization

pulses from -90 mV holding potential (HP) to test potentials ranging from -50 mV to +60 (10 mV step) at 10-second intervals. $I_{Ca\text{-}T}$ was elicited by 250 ms depolarizing pluses (10 mV step) from a HP of -90 mV to +60 mV**.** For I_{Na} recordings, external solution contained (in mM): 60 N-Methyl glucosamine, 60 NaCl, 10 CsCl, 1.8 $CaCl_2$, 1 $MgCl_2$, 10 HEPES, and 10 glucose (pH=7.4, with CsOH). $I_{Ca\text{-}L}$ and $I_{Ca\text{-}T}$ were blocked by $CoCl_2$ (5 mM) and $NiCl_2$ (1 mM), respectively. The internal solution contained (mM) 135 CsOH, 135 L-aspartic acid, 1 $MgCl_2$, 10 EGTA, 10 HEPES, 5 Mg-ATP, and 0.1 Na-GTP (pH 7.2, CsOH). I_{Na} was evoked with 30 ms duration pulses to +30 mV from a HP of -90 mV at 5-second intervals.

For K^+ currents family, the extracellular solution was adjusted as follows. For the classic delayed rectifier current (I_K), 4-AP (0.5 mM) and verapamil (10 μM) was used to block the transient outward current (I_{to}), and $I_{Ca\text{-}L}$ respectively. I_K was elicited by step membrane depolarization from -50 mV to +60 mV. I_{to} was studied in the presence of TEA-Cl and $CdCl_2$ (200 μM) and current was elicited by step depolarization from -50 mV to +60 mV. The pacemaker current (I_f) was studied by adding $BaCl_2$ (1 mM) to the external solution and the membrane was then hyperpolarized from -20 mV to -130 mV. The standard pipette solution contained (mM): 110 K-aspartate, 20 KCl, 2 $CaCl_2$, 1 $MgCl_2$, 0.1 GTP, 5 Mg_2-ATP, 5 Na_2-phosphocreatine, EGTA 10, and HEPES 10, (pH=7.3, with KOH). Data were sampled with an A/D converter (Digital 1320A, Axon Instruments) and stored on the hard disk of a computer for subsequent analysis. Data were acquired by using PCLAMP 8.0 software (Axon Instruments, Union City, CA) and analyzed with ORIGIN 7.0 software (OriginLab, Northampton, MA) and CLAMPFIT 8.2 (Axon Instruments).

References

1. Brillantes AB, Ondrias K, Scott A, Kobrinsky E, Ondriasova E, Moschella MC, Jayaraman T, Landers M, Ehrlich BE, Marks AR. Stabilization of calcium release channel (ryanodine receptor) function by FK506-binding protein. *Cell*. 1994;77:513-23.
2. Marx SO, Gaburjakova J, Gaburjakova M, Henrikson C, Ondrias K, Marks AR. Coupled gating between cardiac calcium release channels (ryanodine receptors). *Circ Res*. 2001;88:1151-8.
3. Marx SO, Reiken S, Hisamatsu Y, Jayaraman T, Burkhoff D, Rosemblit N, Marks AR. PKA phosphorylation dissociates FKBP12.6 from the calcium release channel (ryanodine receptor): defective regulation in failing hearts. *Cell*. 2000;101:365-76.
4. Priori SG, Napolitano C, Tiso N, Memmi M, Vignati G, Bloise R, Sorrentino V, Danieli GA. Mutations in the cardiac ryanodine receptor gene (hRyR2) underlie catecholaminergic polymorphic ventricular tachycardia. *Circulation*. 2001;103:196-200.
5. Laitinen PJ, Brown KM, Piippo K, Swan H, Devaney JM, Brahmbhatt B, Donarum EA, Marino M, Tiso N, Viitasalo M, Toivonen L, Stephan DA, Kontula K. Mutations of the cardiac ryanodine receptor (RyR2) gene in familial polymorphic ventricular tachycardia. *Circulation*. 2001;103:485-90.
6. Bauce B, Rampazzo A, Basso C, Bagattin A, Daliento L, Tiso N, Turrini P, Thiene G, Danieli GA, Nava A. Screening for ryanodine receptor type 2 mutations in families with effort-induced polymorphic ventricular arrhythmias and sudden death: early diagnosis of asymptomatic carriers. *J Am Coll Cardiol*. 2002;40:341-9.
7. Tiso N, Stephan DA, Nava A, Bagattin A, Devaney JM, Stanchi F, Larderet G, Brahmbhatt B, Brown K, Bauce B, Muriago M, Basso C, Thiene G, Danieli GA, Rampazzo A. Identification of mutations in the cardiac ryanodine receptor gene in families affected with arrhythmogenic right ventricular cardiomyopathy type 2 (ARVD2). *Hum Mol Genet*. 2001;10:189-94.
8. Priori SG, Napolitano C, Memmi M, Colombi B, Drago F, Gasparini M, DeSimone L, Coltorti F, Bloise R, Keegan R, Cruz Filho FE, Vignati G, Benatar A, DeLogu A. Clinical and molecular characterization of patients with catecholaminergic polymorphic ventricular tachycardia. *Circulation*. 2002;106:69-74.
9. Lehnart SE, Wehrens XH, Laitinen PJ, Reiken SR, Deng SX, Cheng Z, Landry DW, Kontula K, Swan H, Marks AR. Sudden death in familial polymorphic ventricular tachycardia associated with calcium release channel (ryanodine receptor) leak. *Circulation*. 2004;109:3208-14.
10. Swan H, Piippo K, Viitasalo M, Heikkila P, Paavonen T, Kainulainen K, Kere J, Keto P, Kontula K, Toivonen L. Arrhythmic disorder mapped to chromosome 1q42-q43 causes malignant polymorphic ventricular tachycardia in structurally normal hearts. *J Am Coll Cardiol*. 1999;34:2035-42.
11. Marks AR, Priori S, Memmi M, Kontula K, Laitinen PJ. Involvement of the cardiac ryanodine receptor/calcium release channel in catecholaminergic polymorphic ventricular tachycardia. *J Cell Physiol*. 2002;190:1-6.

12. Corrado D, Basso C, Thiene G, McKenna WJ, Davies MJ, Fontaliran F, Nava A, Silvestri F, Blomstrom-Lundqvist C, Wlodarska EK, Fontaine G, Camerini F. Spectrum of clinicopathologic manifestations of arrhythmogenic right ventricular cardiomyopathy/dysplasia: a multicenter study. *J Am Coll Cardiol*. 1997;30:1512-20.
13. Wehrens XH, Lehnart SE, Huang F, Vest JA, Reiken SR, Mohler PJ, Sun J, Guatimosim S, Song LS, Rosemblit N, D'Armiento JM, Napolitano C, Memmi M, Priori SG, Lederer WJ, Marks AR. FKBP12.6 deficiency and defective calcium release channel (ryanodine receptor) function linked to exercise-induced sudden cardiac death. *Cell*. 2003;113:829-40.
14. Franzini-Armstrong C, Protasi F, Ramesh V. Shape, size, and distribution of Ca(2+) release units and couplons in skeletal and cardiac muscles. *Biophys J*. 1999;77:1528-39.
15. Shannon TR, Pogwizd SM, Bers DM. Elevated sarcoplasmic reticulum Ca2+ leak in intact ventricular myocytes from rabbits in heart failure. *Circ Res*. 2003;93:592-4.
16. Ito K, Shigematsu S, Sato T, Abe T, Li Y, Arita M. JTV-519, a novel cardioprotective agent, improves the contractile recovery after ischaemia-reperfusion in coronary perfused guinea-pig ventricular muscles. *Br J Pharmacol*. 2000;130:767-76.
17. Hachida M, Kihara S, Nonoyama M, Koyanagi H. Protective effect of JTV519, a new 1,4-benzothiazepine derivative, on prolonged myocardial preservation. *J Card Surg*. 1999;14:187-93.
18. Kawabata H, Nakagawa K, Ishikawa K. A novel cardioprotective agent, JTV-519, is abolished by nitric oxide synthase inhibitor on myocardial metabolism in ischemia-reperfused rabbit hearts. *Hypertens Res*. 2002;25:303-9.
19. Wehrens XH, Lehnart SE, Reiken SR, Deng SX, Vest JA, Cervantes D, Coromilas J, Landry DW, Marks AR. Protection from cardiac arrhythmia through ryanodine receptor-stabilizing protein calstabin2. *Science*. 2004;304:292-6.
20. Laurita KR, Girouard SD, Rosenbaum DS. Modulation of ventricular repolarization by a premature stimulus. Role of epicardial dispersion of repolarization kinetics demonstrated by optical mapping of the intact guinea pig heart. *Circ Res*. 1996;79:493-503.
21. Berlin JR, Cannell MB, Lederer WJ. Cellular origins of the transient inward current in cardiac myocytes. Role of fluctuations and waves of elevated intracellular calcium. *Circ Res*. 1989;65:115-26.
22. Goldhaber JI, Xie LH, Duong T, Motter C, Khuu K, Weiss JN. Action potential duration restitution and alternans in rabbit ventricular myocytes: the key role of intracellular calcium cycling. *Circ Res*. 2005;96:459-66.
23. Chudin E, Goldhaber J, Garfinkel A, Weiss J, Kogan B. Intracellular Ca(2+) dynamics and the stability of ventricular tachycardia. *Biophys J*. 1999;77:2930-41.
24. Cerrone M, Colombi B, Santoro M, di Barletta MR, Scelsi M, Villani L, Napolitano C, Priori SG. Bidirectional ventricular tachycardia and fibrillation elicited in a knock-in mouse model carrier of a mutation in the cardiac ryanodine receptor. *Circ Res*. 2005;96:e77-82.

25. Kollmar R, Montgomery LG, Fak J, Henry LJ, Hudspeth AJ. Predominance of the alpha1D subunit in L-type voltage-gated Ca2+ channels of hair cells in the chicken's cochlea. *Proc Natl Acad Sci U S A*. 1997;94:14883-8.
26. Koschak A, Reimer D, Huber I, Grabner M, Glossmann H, Engel J, Striessnig J. alpha 1D (Cav1.3) subunits can form l-type Ca2+ channels activating at negative voltages. *J Biol Chem*. 2001;276:22100-6.
27. Matthes J, Yildirim L, Wietzorrek G, Reimer D, Striessnig J, Herzig S. Disturbed atrio-ventricular conduction and normal contractile function in isolated hearts from Cav1.3-knockout mice. *Naunyn Schmiedebergs Arch Pharmacol*. 2004;369:554-62.
28. Zhang Z, He Y, Tuteja D, Xu D, Timofeyev V, Zhang Q, Glatter KA, Xu Y, Shin HS, Low R, Chiamvimonvat N. Functional roles of Cav1.3(alpha1D) calcium channels in atria: insights gained from gene-targeted null mutant mice. *Circulation*. 2005;112:1936-44.
29. Qu Y, Baroudi G, Yue Y, Boutjdir M. Novel molecular mechanism involving alpha1D (Cav1.3) L-type calcium channel in autoimmune-associated sinus bradycardia. *Circulation*. 2005;111:3034-41.
30. Mangoni ME, Couette B, Bourinet E, Platzer J, Reimer D, Striessnig J, Nargeot J. Functional role of L-type Cav1.3 Ca2+ channels in cardiac pacemaker activity. *Proc Natl Acad Sci U S A*. 2003;100:5543-8.
31. Yue L, Feng J, Gaspo R, Li GR, Wang Z, Nattel S. Ionic remodeling underlying action potential changes in a canine model of atrial fibrillation. *Circ Res*. 1997;81:512-25.
32. Van Wagoner DR, Pond AL, Lamorgese M, Rossie SS, McCarthy PM, Nerbonne JM. Atrial L-type Ca2+ currents and human atrial fibrillation. *Circ Res*. 1999;85:428-36.
33. Lai LP, Su MJ, Lin JL, Lin FY, Tsai CH, Chen YS, Huang SK, Tseng YZ, Lien WP. Down-regulation of L-type calcium channel and sarcoplasmic reticular Ca(2+)-ATPase mRNA in human atrial fibrillation without significant change in the mRNA of ryanodine receptor, calsequestrin and phospholamban: an insight into the mechanism of atrial electrical remodeling. *J Am Coll Cardiol*. 1999;33:1231-7.
34. Brundel BJ, van Gelder IC, Henning RH, Tuinenburg AE, Deelman LE, Tieleman RG, Grandjean JG, van Gilst WH, Crijns HJ. Gene expression of proteins influencing the calcium homeostasis in patients with persistent and paroxysmal atrial fibrillation. *Cardiovasc Res*. 1999;42:443-54.
35. Gaborit N, Steenman M, Lamirault G, Le Meur N, Le Bouter S, Lande G, Leger J, Charpentier F, Christ T, Dobrev D, Escande D, Nattel S, Demolombe S. Human atrial ion channel and transporter subunit gene-expression remodeling associated with valvular heart disease and atrial fibrillation. *Circulation*. 2005;112:471-81.
36. Xu W, Lipscombe D. Neuronal Ca(V)1.3alpha(1) L-type channels activate at relatively hyperpolarized membrane potentials and are incompletely inhibited by dihydropyridines. *J Neurosci*. 2001;21:5944-51.
37. Namkung Y, Skrypnyk N, Jeong MJ, Lee T, Lee MS, Kim HL, Chin H, Suh PG, Kim SS, Shin HS. Requirement for the L-type Ca(2+) channel alpha(1D) subunit in postnatal pancreatic beta cell generation. *J Clin Invest*. 2001;108:1015-22.